AD-A036 000 IRT CORP SAN DIEGO CALIF F/G 14/2
EVALUATION OF CALIFORNIUM-252-BASED NEUTRON RADIOGRAPHY AND PHO--ETC(U)
AUG 76 H HARPER, J C YOUNG, J BALTGALVIS DAAJ01-75-C-0895
UNCLASSIFIED IRT-6102-003 USAAVSCOM-TR-76-24 NL

1 OF 1
AD
A036000

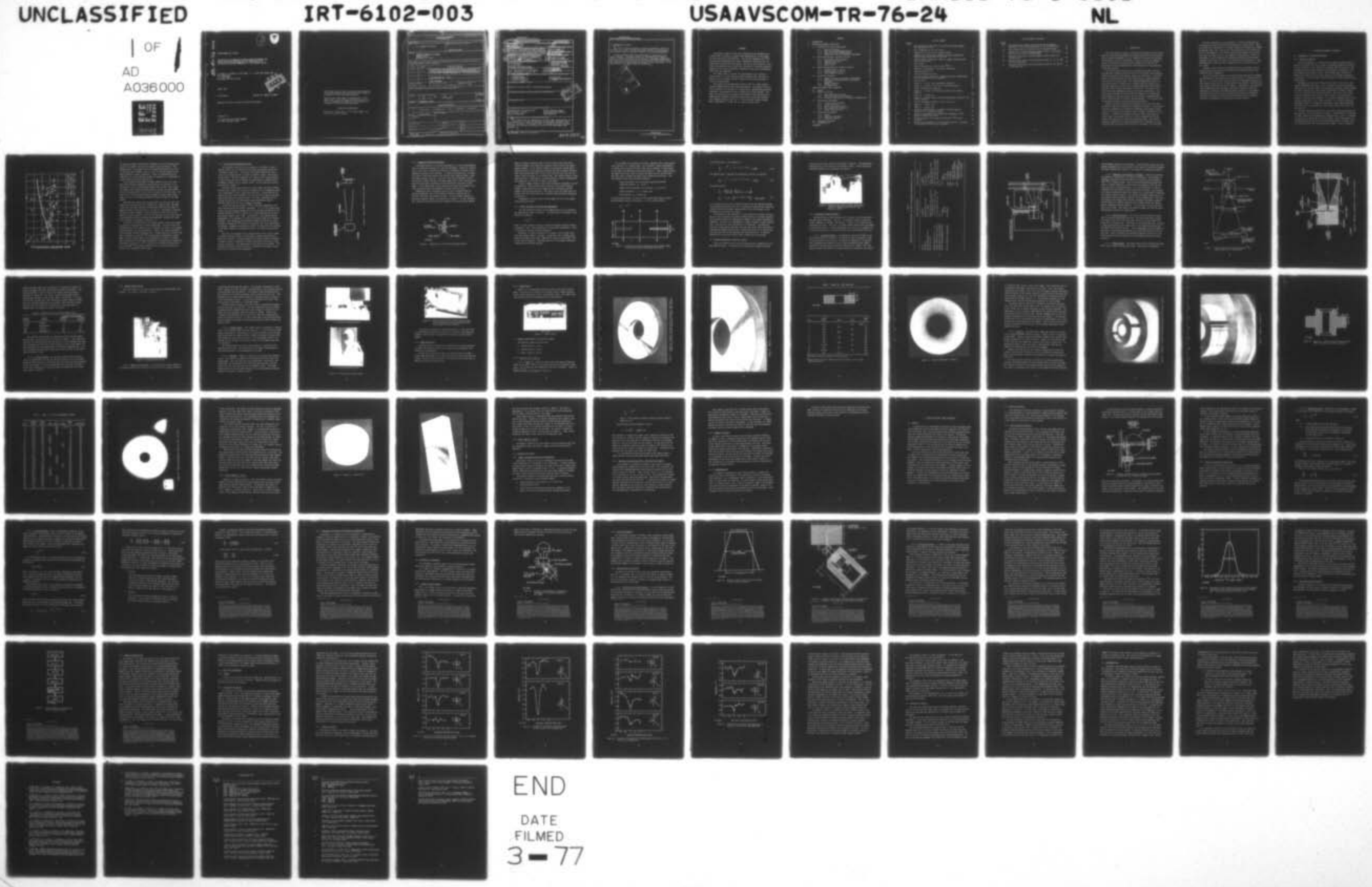

END
DATE
FILMED
3-77


1.0
1.1
1.25
1.4
1.6
1.8
2.0
2.2
2.5
2.8
3.2
3.6
4.0
4.5
5.0
5.6
6.3
7.1

AD-A036 000

2
B.S.

AVSCOM REPORT NO. TR76-24

EVALUATION OF CALIFORNIUM-252-BASED NEUTRON RADIOGRAPHY AND PHOTON SCATTERING TECHNIQUES FOR THE INSPECTION OF HOT ISO-STATICALLY PRESSED COMPONENTS OF T-700 AIRCRAFT ENGINE

H. Harper, J. Baltgalvis, Hans Weber, J. C. Young, and Joseph John
IRT Corporation
P. O. Box 80817
San Diego, California 92138

August 1976

Final Report

Contract No. DAAJ01-75-C-0895

Approved for public release; distribution unlimited

Prepared for

U.S. ARMY AVIATION SYSTEMS COMMAND
St. Louis, Missouri 63166

DISPOSITION INSTRUCTIONS

Destroy this report when it is no longer needed. Do not return to the originator.

REQUEST FOR SHIPMENT

(AVSCOM Reg 55-9)

Submit in triplicate.

TO:	FROM: *(Specify Dir/Ofc and Office Symbol)*
CHIEF, PASSENGER DIVISION, H&ISA	DRSAV-ZDR (BOYD)

SHIP TO:

DEFENSE DOCUMENTATION CENTER
CAMERON STATION
ARLINGTON, VA 22314

SPECIAL NOTE: *If shipment is estimated to be within Parcel Post limitations (40 lbs; 72 inches, combined length and girth) requester will prepare the shipping label (DA Label 18) for each package.*

ITEM NO	QUANTITY *(each)*	DESCRIPTION OF ARTICLES *(Include NSN, if applicable.)*
1	2	EVALUATION OF CALIFORNIUM-252-BASED NEUTRON RADIOGRAPHY AND PHOTON SCATTERING TECHNIQUES FOR THE INSPECTION OF HOT ISO-STATICALLY PRESSED COMPONENTS OF T-700 AIRCRAFT ENGINE.
		USAAVSCOM RPT NO. 76-24
		(DDC SHIPMENT)

METHOD OF SHIPMENT	SPECIFY *(If service is required)*	REQUIRED DELIVERY DATE *(Julian Date)*
[X] PREPAID [ ] COLLECT	[ ] CERTIFIED MAIL [ ] REGISTERED MAIL	7706

SPECIAL CONDITIONS INFLUENCING ROUTING - *(Specify if hazardous, classified, fragile, etc.)*

DATE OF REQUEST	SIGNATURE OF REQUESTER	TELEPHONE EXTENSION
8 FEB 77	Binette W. Boyd BINETTE W. BOYD	3764

TRANSPORTATION USE ONLY

SHIPPED VIA: [ ] PARCEL POST [ ] AIR PARCEL POST [ ] MOM [ ] CERTIFIED [ ] REGISTERED

[ ] COMMON CARRIER — NAME OF CARRIER

GBL NO

NUMBER CTN/BX	WEIGHT	CUBE
PACKED BY		DATE
SHIPPED BY		DATE

SAV Form 1 Aug 74 689 — Edition of 1 Nov 72, may be used.

UNCLASSIFIED

SECURITY CLASSIFICATION OF THIS PAGE (When Data Entered)

18 19

REPORT DOCUMENTATION PAGE		READ INSTRUCTIONS BEFORE COMPLETING FORM
1. REPORT NUMBER US AVSCOM TR76-24	2. GOVT ACCESSION NO.	3. RECIPIENT'S CATALOG NUMBER 9
4. TITLE (and Subtitle) 6 EVALUATION OF CALIFORNIUM-252-BASED NEUTRON RADIOGRAPHY AND PHOTON SCATTERING TECHNIQUES FOR THE INSPECTION OF HOT ISO-STATICALLY PRESSED COMPONENTS OF T-700 AIRCRAFT ENGINE.		5. TYPE OF REPORT & PERIOD COVERED Final Report,
		6. PERFORMING ORG. REPORT NUMBER 14 IRT-6102-003
7. AUTHOR(s) 10 H. Harper, J. Baltgalvis, Hans Weber, J. C. Young [redacted] Joseph John		8. CONTRACT OR GRANT NUMBER(s) 15 DAAJ01-75-C-0895 New
9. PERFORMING ORGANIZATION NAME AND ADDRESS IRT Corporation P. O. Box 80817 San Diego, California 92138		10. PROGRAM ELEMENT, PROJECT, TASK AREA & WORK UNIT NUMBERS PEM Project 1757096 AMCMS Code: 1497.94.5. S7096(XZ5)
11. CONTROLLING OFFICE NAME AND ADDRESS U. S. Army Aviation Systems Command ATTN: DRSAV-PUEB, P. O. Box 209 St. Louis, Missouri 63166		12. REPORT DATE 11 Aug[redacted] [redacted]76
		13. NUMBER OF PAGES 82
14. MONITORING AGENCY NAME & ADDRESS(if different from Controlling Office) 12 84p.		15. SECURITY CLASS. (of this report) Unclassified
		15a. DECLASSIFICATION/DOWNGRADING SCHEDULE

16. DISTRIBUTION STATEMENT (of this Report)

Approved for public release; distribution unlimited.

17. DISTRIBUTION STATEMENT (of the abstract entered in Block 20, if different from Report)

18. SUPPLEMENTARY NOTES

19. KEY WORDS (Continue on reverse side if necessary and identify by block number)

Nondestructive Testing Techniques	Photon Scattering Gauge
Hot Iso-Static Pressing	Three-Dimensional Response
Neutron Radiography	High Resolution

20. ABSTRACT (Continue on reverse side if necessary and identify by block number)

The evaluation of two nondestructive testing (NDT) techniques for the flaw inspection of turbine disk material for the General Electric T-700 engine is described. The material which is produced by the Hot Iso-Static Pressing (HIP) technique introduces a new set of NDT requirements and problems.

DD FORM 1 JAN 73 1473 EDITION OF 1 NOV 65 IS OBSOLETE

409 388 LB

20. ABSTRACT (Continued)

The first technique evaluated is neutron radiographic inspection. It proves to be capable of detecting flaws; however, a certain degree of development work is required to improve its resolution capability.

A newly developed Photon Scattering Gauge is evaluated as the second technique. Although tailored for the inspection of explosive filler in 105-mm projectiles, the existing test instrument demonstrates the feasibility of the technique for the inspection of HIP turbine parts. The response of the Photon Scattering Gauge is three dimensional. It is characterized by its high-resolution capability.

FOREWORD

The subject report describes the evaluation of two nondestructive testing (NDT) techniques as regards their applicability to the problem of flaw inspection in HIP materials. The two NDT techniques are ^{252}Cf-based neutron radiography and filmless radiometric inspection with IRT Corporation's photon scattering gauge. The latter was included as a most recent development which had just been subjected to a thorough parametric analysis by the time a preliminary evaluation of the neutron radiographic effort had been completed.

The author wishes to express his appreciation to Mr. Anthony C. Piazza of the U. S. Army Aviation Systems Command and Mr. Don Nulk of General Electric Company for their interest in this work expressed in stimulating discussions.

This project was accomplished as part of the U. S. Army Aviation Systems Command Manufacturing Technology program. The primary objective of this program is to develop, on a timely basis, manufacturing processes, techniques, and equipment for use in production of Army material. Comments are solicited on the potential utilization of the information contained herein as applied to present and/or future production programs. Such comments should be sent to: U. S. Army Aviation Systems Command, ATTN: DRSAV-PUEB, P. O. Box 209, St. Louis, Missouri 63166.

CONTENTS

LIST OF FIGURES

LIST OF FIGURES (Continued)

1. INTRODUCTION

The effort under the subject contract was undertaken with the initial objective of providing equipment and engineering services for the evaluation of neutron-radiographic (n-ray) inspection of turbine disk material for the General Electric T-700 engine. Later, the scope was widened to include a preliminary evaluation of the feasibility of applying IRT Corporation's newly developed photon scattering gauge to the inspection of the same material.

The T-700 turbine disk material is produced by the Hot Isostatic Pressing (HIP) technique with the objective of providing a more suitable turbine disk material with greater overall cost efficiency. In the HIP process tiny powder grains are made by breaking up a stream of molten metal with jets of inert argon. The resulting homogeneous mixture of the various metals is cleaned of the residual argon and placed in an evacuated enclosure in an autoclave at high temperatures and pressures, typically 1800 to 2200°F and 10,000 to 30,000 psi. The result is an alloy with a more homogeneous mixture of the metal constituents. One of the main advantages of the HIP material compared to a conventional metal forging is that the original part can be made to dimensions more nearly those required of the final finished product. This decreases cost by reducing the amount of waste material and machining.

However, the goal of initially producing a part to the near final dimensions creates new nondestructive inspection problems. In particular, ultrasonic techniques are incapable of examining a skin depth of about 1 mm at the surface of the material, due to inherent limitations of this technique. A problem of ultrasonic inspection which can probably be solved, even if with great difficulty, is the interpretation of echo signals from samples with other than squared-off sides. The need for alternate nondestructive testing techniques for HIP components is thus identified and two possible alternatives are discussed in the following.

The first alternative, n-ray inspection, is based on technology and instrumentation which has been under development for several years. While it has been well established as a powerful inspection technique for a number of problems (Refs 1-12), this was the first application to the inspection of HIP T-700 components. The results indicate that within certain resolution limits for small defects n-ray inspection does provide a useful tool. Furthermore, it can be improved by developing techniques and instrument components specifically tailored to the inspection of HIP materials. Such improvements are listed but their implementation was outside the scope of this effort.

Instead, a brief study was undertaken to take a preliminary look at the applicability of the newly developed Photon Scattering Gauge to the inspection of HIP components.

The first and only system of this kind had been specifically designed and configured for the inspection of explosive filler in 105-mm projectiles (Ref 13). It was tailored to meet the inspection requirements peculiar to that problem, and was not at all optimized for the geometric and resolution requirements associated with the HIP samples. Nevertheless, the inspection results demonstrate that the photon scattering technique is feasible. Importantly, a previously performed parametric analysis of the response characterization of the photon scattering gauge permitted a parametric projection to be made to a system which would meet the very stringent resolution requirements for the detection of minute defects.

2. NEUTRON-RADIOGRAPHIC INSPECTION

2.1 FUNDAMENTALS OF NEUTRON RADIOGRAPHY

2.1.1 Physical Principle

Neutron radiography is a nondestructive inspection technique that is similar in principle to x ray, in that a penetrating radiation (neutrons) is used to obtain a visual image of the internal form of an object. The transmitted neutron beam is detected and permanently recorded on a suitable imaging system (usually film). The recorded image represents a shadow of the object, with the lower density on the image corresponding to portions of the object that are more effective in attenuating the direct neutron beam.

Although n-ray and x-ray techniques are similar in principle, they actually complement each other. This is because the relative absorption characteristics of most elements are essentially reversed; thermal neutrons are highly attenuated by light elements (principally hydrogen), whereas x rays are attenuated more by heavy elements. Thus with n rays, nondestructive inspection can be made of light elements or certain defects encased in or behind heavy elements. It can detect imperfections in thick samples through which x rays cannot penetrate, or in samples containing hydrogenous matter or contaminants (penetrants) whose neutron-absorbing and neutron-scattering properties differ significantly from those of the base material.

The mass absorption coefficients of naturally occurring elements for neutrons and x rays are displayed in Figure 1. When plotted as a function of atomic number, the mass absorption coefficient for x rays is a smoothly varying function increasing with atomic number. On the other hand, the corresponding values for n rays fluctuate from element to element, and on the average decrease with increasing atomic number. Hence, in general,

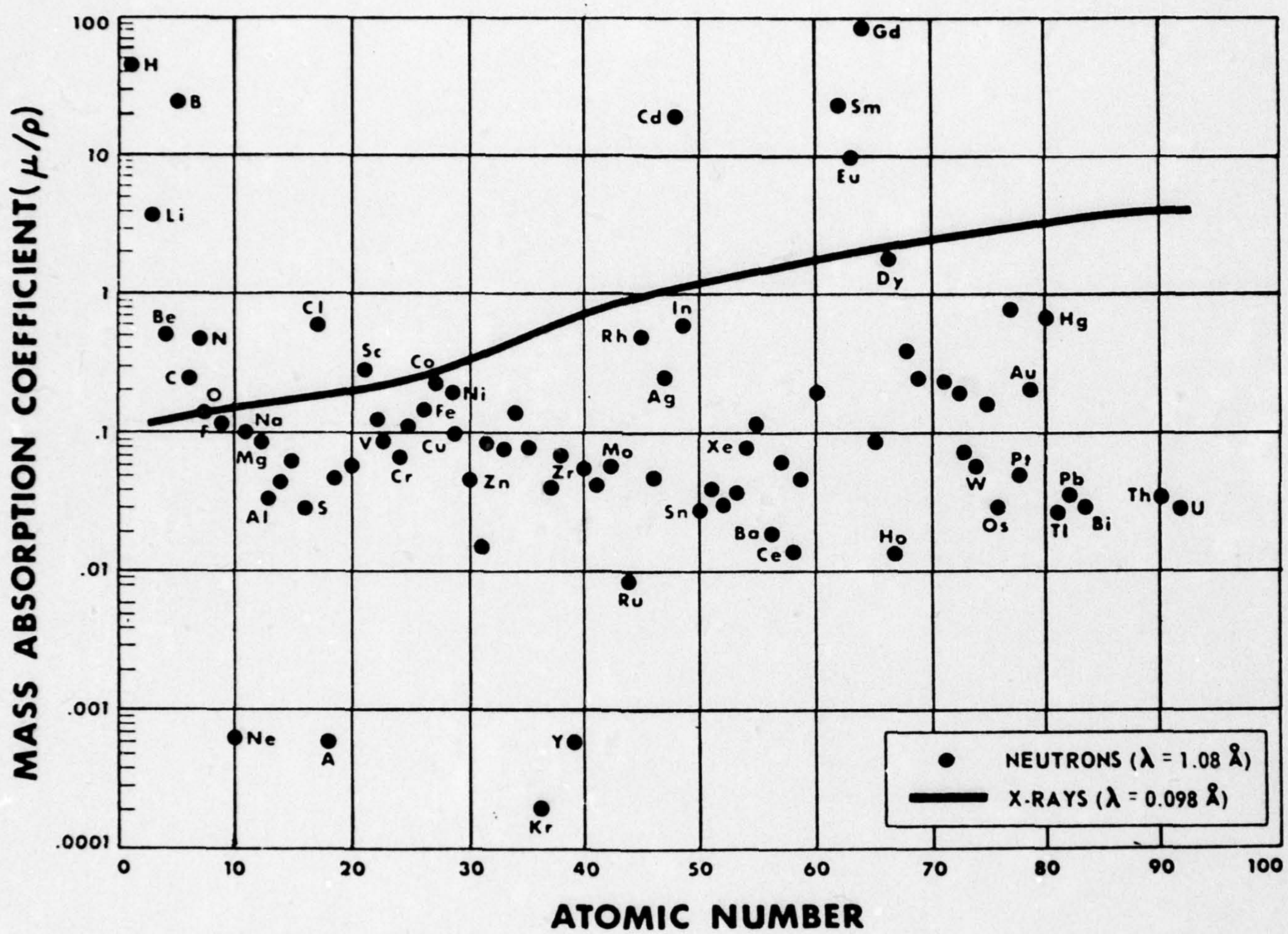

Figure 1. Mass absorption coefficients of naturally occurring elements for neutrons and x rays

the lightest elements (particularly hydrogen), are the most opaque and the heavier elements are the least opaque to thermal neutrons. This characteristic is the opposite of the attenuation properties of x rays in which the heavy elements, such as lead, are the most opaque and the light elements are quite transparent. Hence, by complementing x-ray inspection, the n-ray technique extends the capability of radiography to a much broader spectrum of applications.

Since elements which differ in atomic number by only a few units have widely differing absorption characteristics for neutrons, it is possible for n rays to distinguish between them, whereas x rays cannot. For example, mass absorption coefficients for nickel and copper differ by only a few percent for x rays, but by a factor of two for n rays. Not only can an n ray distinguish between elements of nearly equal atomic number, it can even distinguish between different isotopes of the same element.

Of particular interest for this application is the fact that a few elements, for example boron (B), cadmium (Cd), samarium (Sm), and gadolinium (Gd), have mass absorption coefficients which are two orders of magnitude greater than those for Fe, Ni, and Cu. Consequently, penetrant solutions of these elements, if the solutions can find access to the defects, provide a powerful assist for the detection of even small defects. A detailed description of the penetrant enhancement technique for detection of defects is presented in Section 2.1.4.

In the past the availability of suitable neutron sources has limited the growth and application of neutron radiography. Nuclear reactors and accelerators which are commonly used are expensive to acquire, are troublesome to maintain, and lack portability. However, the recent availability of the man-made isotope Californium-252, a copious emitter of neutrons, has made it feasible to construct ^{252}Cf-based neutron radiographic systems, which, because of their lower cost and portability, promise to significantly expand the use of neutron radiography for nondestructive inspection. The neutron yield of 2.3×10^{12} n/sec/g and its radioactive half-life at 2.65 years make ^{252}Cf uniquely suited for use as a practical source of neutrons for radiographic applications.

2.1.2 Basic Neutron-Radiography System

The important function of n-ray systems is to achieve as large a thermal-neutron flux as possible at the object and imaging system with a minimum of gamma rays. In addition, the thermal-neutron flux must arrive at the imaging plane in a beam to produce a sharp, clear picture of the object. The basic components of a typical n-ray system required to realize these objectives comprise a neutron source, a moderator and collimator assembly, and an imaging system. Such an idealized system is illustrated in Figure 2.

The ideal neutron source would be a point source that emits thermal neutrons with a large flux and source strength with no accompanying gamma rays; unfortunately, such a source does not exist. Californium-252 is a radioactive source that overcomes, for the first time, some of the fundamental deficiencies of neutron sources. Its basic characteristics of intense neutron activity with minimal gamma contamination make it extremely attractive for use in neutron radiography.

As the best source available, ^{252}Cf is the best compromise on the ideal neutron source for neutron radiography. It is a very intense point source with relatively few gamma rays, but the energy distribution of the neutrons emitted by ^{252}Cf is similar to a fission spectrum with an average neutron energy of over 1 MeV. Consequently, to do thermal-neutron radiography, it is necessary to reduce the average energy of the neutron spectrum. This moderation of the neutron energy distribution is accomplished by placing the ^{252}Cf source in a material that has a high density of hydrogen. Hydrogen has the unique ability of slowing down the neutrons in the fewest number of scattering collisions, and thus in the smallest volume.

Now that we are forced to use a neutron source with a finite volume to generate thermal neutrons, we must define a neutron beam from the source to the object. The source looks at the object through a divergent collimator, which is selected to maximize the neutron flux over as wide an area as possible. The image plane is the location of the object. The imaging system must be placed as close as possible to the object to produce clear, high-resolution radiographs.

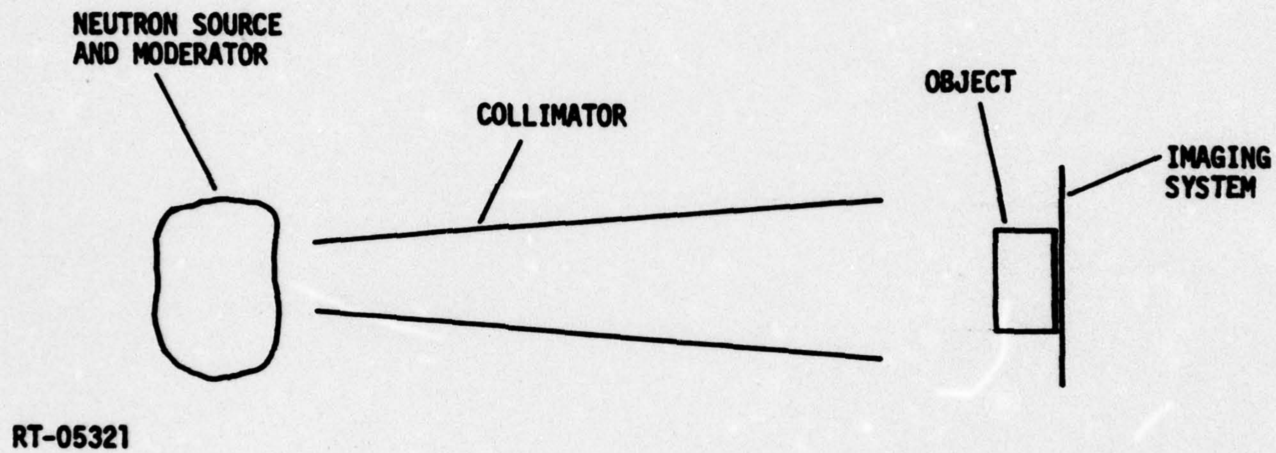

Figure 2. Basic components of an n-ray system

2.1.3 Imaging for Neutron Radiography

The general practice in neutron radiography is to utilize photographic film as a penetrant recording of a neutron radiograph. Unlike the situation with x rays, film is relatively insensitive to neutrons, and hence, direct imaging by neutrons is not feasible. To improve the sensitivity, a converter screen is used that captures the neutrons and ultimately emits a radiation that activates the film. Converters fall into two general classes: (1) metallic screens that emit low-energy gamma rays, x rays, and electrons, and (2) scintillators (loaded with neutron absorbers) that emit visible light. As one would expect, metal converters are used with standard x-ray film, and scintillators are employed with light-sensitive film.

Depending on the circumstances and the type of converter used for neutron radiography, one of two different methods of exposure may be utilized--the direct and transfer methods. The most common technique is the direct-exposure method, as illustrated in Figure 3. In this technique, the converter screen and the film are exposed to the neutron beam together.

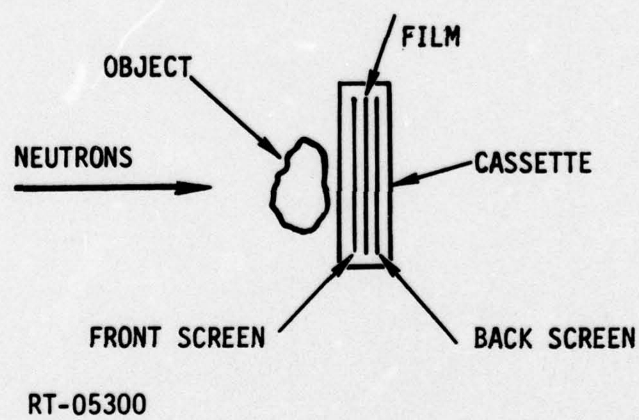

Figure 3. Imaging for n ray by direct exposure method

Some of the metal converters and all of the scintillators emit their radiation promptly upon capturing a neutron, and are used in the direct-exposure method. In the transfer method, one uses metal screens which become radioactive upon capturing a neutron, and emit a delayed radiation. Since this delayed radiation is used to activate the film, only the converter screen is exposed to the neutron beam. The transfer method is used when the object is radioactive, the neutron beam is severely contaminated with gamma rays, or the best contrast is desirable.

The most common converter screen used in neutron radiography is based on gadolinium. These screens can be used only in the direct-exposure method, as gadolinium emits soft gamma rays and low-energy electrons promptly upon capturing neutrons. When using a very thin gadolinium converter, less than 0.002 inch thick, extremely high-resolution radiographs are possible.

Photographic films are used to record images in all of the imaging systems described above.

2.1.4 Defect Detection with Penetrant Enhancement

For this evaluation effort, we have employed the use of a penetrant for enhancing the areas of interest. A neutron beam is attenuated in any material according to

$$I = I_o e^{-\Sigma t} \quad ,$$

where I is the radiation intensity transmitted through a material having a thickness t and a linear absorption or attenuation coefficient Σ, and I_o is the initial incident radiation intensity.

Naturally, it would be desirable to increase Σ for the path along which the desired defect is located. A penetrant such as $Gd(NO_3)_3 \cdot 6H_2O$ serves this purpose quite well, depending of course on the absolute size of the voids in question. Gadolinium has one of the highest attenuation coefficients for thermal neutrons.

As an example of the benefits of using a penetrant with a high capture cross section, e.g., $Gd(NO_3)_3 \cdot 6H_2O$, let us examine a sample approximately 1.2 inches thick, having two holes 0.030 inch in diameter at right angles to the sample and impinging neutron beam (Figure 4). Beam 1 passes through the sample only; beam 2 passes through the sample with an unfilled hole, and beam 3 passes through the sample with a penetrant-filled hole. For this example we have the following parameters:

Total macroscopic cross section for gadolinium nitrate penetrant solution, $\Sigma_T = 70\ cm^{-1}$;

Sample total macroscopic cross section, $\Sigma_T = 0.70\ cm^{-1}$;

Sample thickness, $t_s = 1.2$ inches; and

Hole diameters, $t_h = 0.030$ inch.

As mentioned previously, the ratio of the neutron beam intensity transmitted through a medium of thickness, t, to the initial beam is

$$\frac{I}{I_0} = e^{-\Sigma t} \quad .$$

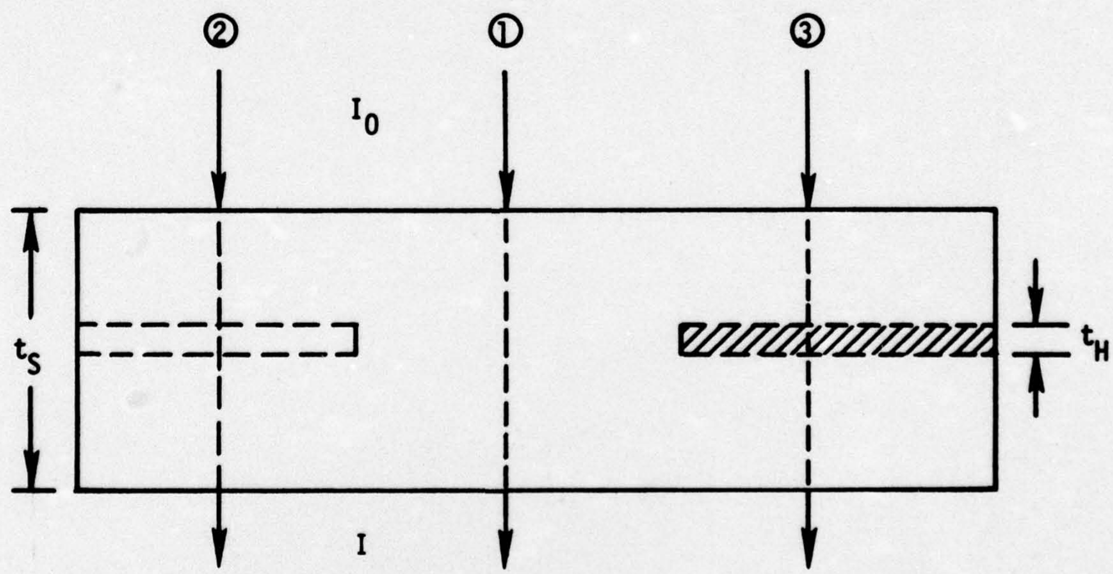

RT-12674

Figure 4. Comparison of neutron beam attenuation through sample with unfilled hole and penetrant-filled hole

For neutron beam 1, this amounts to:

$$\frac{I}{I_0} = e^{-\Sigma t_s} = e^{-0.7 \times 1.2 \times 2.54} = \underline{0.118} \quad . \tag{2.1}$$

For neutron beam 2, ignoring the absorption in the air in the hole:

$$\frac{I}{I_0} = e^{-\ t_s} = e^{-0.7 \times 1.17 \times 2.54} = \underline{0.125} \quad . \tag{2.2}$$

For neutron beam 3:

$$\frac{I}{I_0} = \left(e^{-\Sigma t}_{\text{sample}}\right) \cdot \left(e^{-\Sigma t}_{\text{penetrant in hole}}\right)$$

$$\frac{I}{I_0} = (0.125) \cdot \left(e^{-70 \times 0.030 \times 2.54}\right) = \underline{6.03 \times 10^{-4}} \quad . \tag{2.3}$$

It is obvious from the above absorption ratios that the beam path through the penetrant-filled hole (Eq. 2.3) is much more attenuated and, neglecting internal neutron scattering, should easily be seen with respect to the attenuation for the other two cases.

The solvent for the penetrant is a 50:50 mixture of alcohol and water. This is used to minimize the surface tension effects on the small apertures. One successful method for impregnating a sample is the vacuum impregnation technique. The part to be impregnated is tightly wrapped in heavy aluminum foil in the form of a dish and placed in a vacuum unit. The penetrant solution is then poured completely over the part, after which the system is evacuated and purged several times in order for the air to be removed from the voids and filled with penetrant upon repressurization. To minimize evaporation of the solvent, Mylar tape is placed over the openings.

2.2 NEUTRON-RADIOGRAPHIC INSPECTION SYSTEM

The n-ray system utilized for this study was IRT's commercially available CFNR-10 system. It consists of the neutroscope, image positioning

system, and beam stop, which are illustrated in Figure 5. The performance characteristics of the system are described in Table 1, which include the resolution capabilities and neutron flux density.

Figure 5. CFNR-10 system (left to right) neutroscope (CFNR-10), imaging system (IS-10), and beam stop (BS-10)

2.2.1 Neutroscope (Neutron Camera)

The neutroscope is shown schematically in Figure 6, which illustrates the main camera components. They are: a biological shield, source positioner, moderator, collimator, and shutter. Figure 6 also illustrates the activation port tube. This tube is an added feature which allows performance of activation analysis. During radiographic use, this port is plugged with a solid polyethylene tube to prevent a beam from exiting through this port.

2.2.1.1 Biological Shield. The biological shield which makes up the bulk of the camera (see Figure 5) is required to permit personnel to work in close proximity of the system. The shield is composed of a solid material containing large amounts of water [water-extended polyester (WEP)] mixed with a neutron capturing material like boron or lithium. This combination reduces the number of secondary gamma rays produced by the capture

Table 1

COMPARISON OF DESIGN SPECIFICATIONS AND ACTUAL PERFORMANCE CHARACTERISTICS OF CFNR-10

	Design Specifications	Actual Performance
Source	10 mg ^{252}Cf	10 mg ^{252}Cf
L/D Ratios	Variable from 15 to 80	14.0 to 98.7
Minimum Radiograph Size	14 x 17 inches	14 x 17 inches
Resolution Limit	Better than 0.04 in. for 0.25 in. Thick object at L/D = 18	0.02 in. for 0.25 in. thick object at L/D = 18
Thermal Neutron Flux 0 - 1 eV	1.4×10^4 n/cm^2 -sec at L/D =20	2.46×10^4 n/cm^2-sec at L/D=20
Thermal Neutron Flux 2200 m/sec	1×10^4 n/cm^2-sec at L/D = 20	1.72×10^4 n/cm^2-sec at L/D=20
Cadmium Ratio (fission chamber)	∿17:1	45.7:1
Thermal Neutron/Gamma-Ray Ratio	$\sim 2 \times \frac{10^5\ n}{cm^2\ \text{-mR}}$	$8.13 \times \frac{10^5\ n}{cm^2\ \text{-mR}}$
Dose at Surface of Camera Body	∿50 mrem/hr	Side: 19 mrem/hr. Back: 15 mrem/hr. Top: (Source in stored position) 56 mrem/hr. Front: (Source in stored position) with shutter closed: 22 mrem/hr.

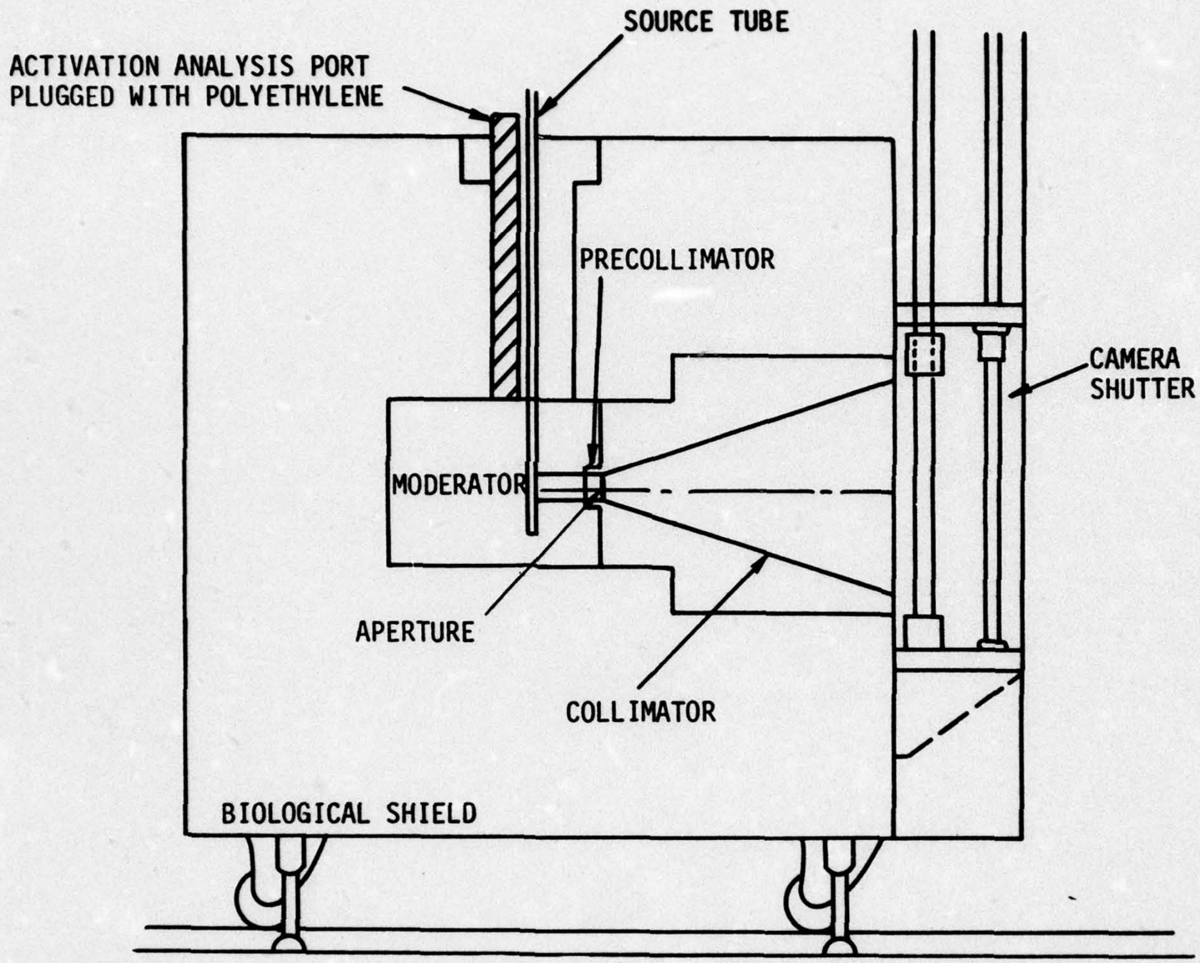

RT-09918

Figure 6. Neutroscope

of the thermal neutrons in the hydrogen. This shielding reduced the total neutron and gamma dose on the surface of the camera to less than 50 mrem/hr. An actual radiation dose profile of the camera is illustrated in Figure 7.

2.2.1.2 Moderator, Precollimator, Collimator. Figure 8 illustrates the moderator, precollimator, collimator, and shutter. The moderator is composed of high-density polyethylene which slows down fission neutrons from ^{252}Cf to thermal energy. Since the entire polyethylene becomes the source of thermal neutrons, an aperture must be defined so that the neutrons can pass to the imaging plane. To do this efficiently, a hole is introduced into the middle of the material near the source. The neutrons exit from the moderator through this aperture to a precollimator consisting of a thermal neutron absorber. This defines the beam by capturing all of the neutrons that may otherwise scatter into the imaging plane. This aperture looks at the imaging plane through a divergent collimator (composed of WEP loaded with lithium carbonate) which further defines the neutron beam by capturing scattered neutrons. A 6-inch piece of lead also forms part of the system. This reduces the number of gamma rays from the source and moderator reaching the imaging plane.

2.2.1.3 Source Positioner. The source positioner moves the source into a stored and radiographic position. The source positioner consists of a crank, cable drive, and source tube which can lock the source into either of its two positions. The source, in the stored position, is inside a lead plug (Figure 8) which reduces most of the radiation exiting from the camera front (shutter closed). In the radiographic position (Figure 8), the source is positioned approximately two inches from the center of the flux trap. Table 2 indicates the encountered radiation levels at 4- and 6-foot distances from the aperture for the different shutter and source positions.

2.2.1.4 Camera Shutter. The camera shutter is the shielded door that blocks the collimator opening when closed. The shutter is composed of

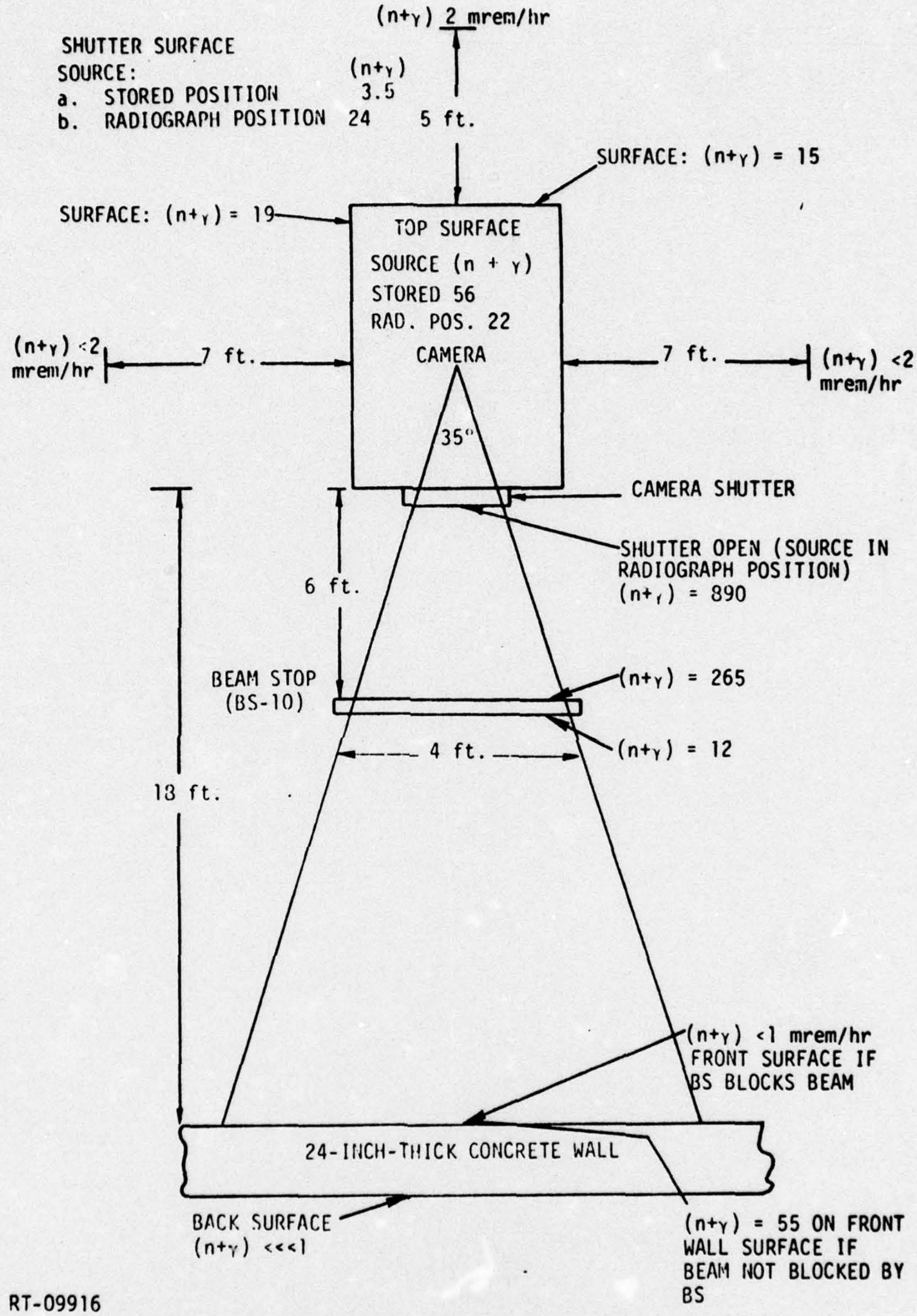

Figure 7. Camera radiation dose profile (10 mg ^{252}Cf) [all values of (n+γ) are mrem/hr]

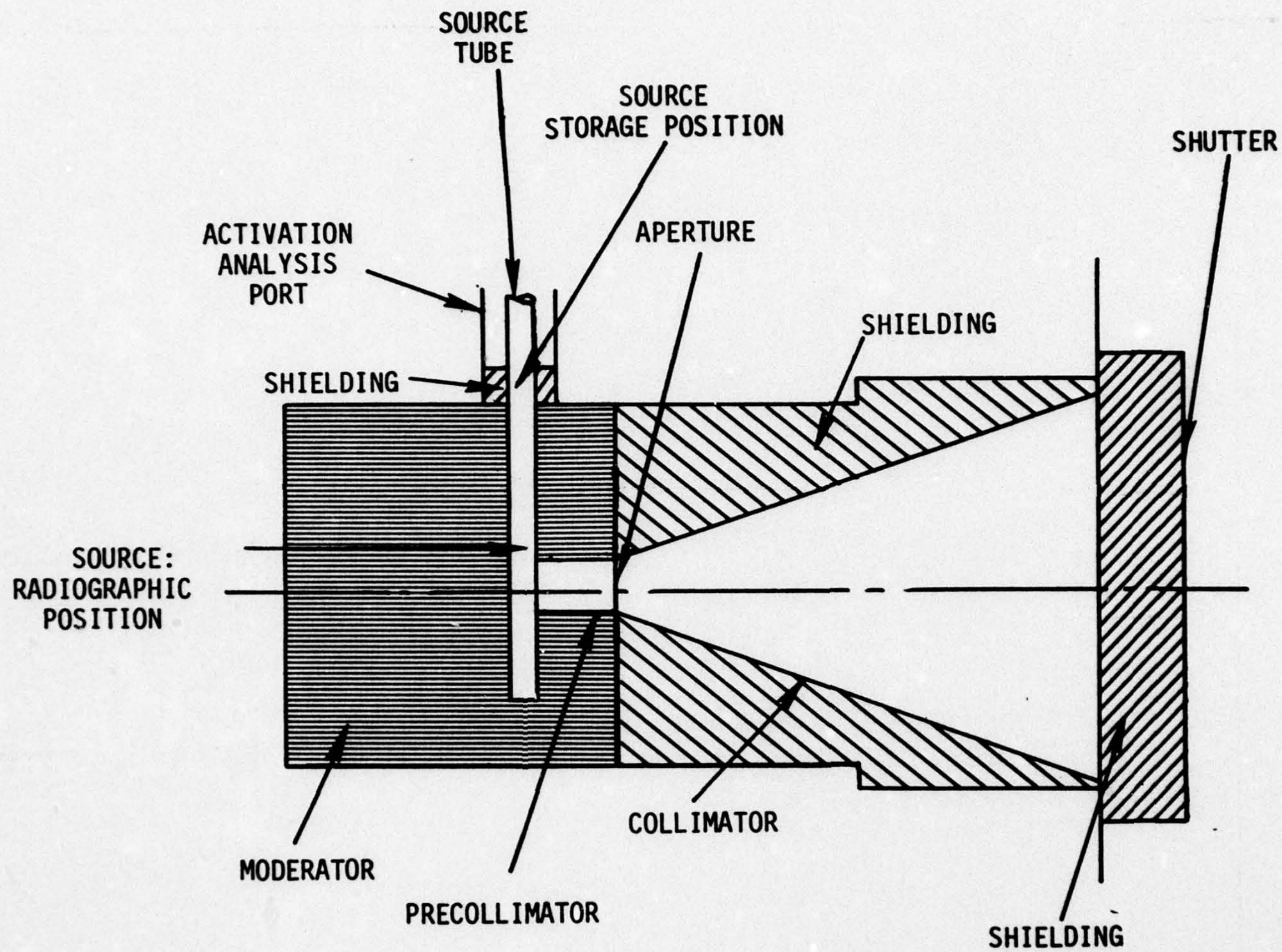

RT-09919

Figure 8. Moderator, precollimator, collimator, and shutter

lithium carbonate, WEP, and lead (Figure 8) to minimize the amount of neutron and gamma radiation exiting from the front of the camera. This enables personnel to work in front of the camera without receiving a large dose of radiation. The shutter is motor driven and has micro switches that indicate, on the control panel, its position. It is controlled from this panel and, when electrically locked, cannot be opened until all interlock conditions are satisfied. When interlock or power failure occurs, the shutter will automatically close and cannot be reopened until the reason for closure is corrected.

Table 2. Radiation Levels in Front of Camera ($n+\gamma$)

Shutter Position	Source Position	Distance from Aperture 4 feet (mrem/hr)	6 feet (mrem/hr)
Closed	Storage	3	1.3
Closed	Radiographic	25	11
Open	Storage	130	58
Open	Radiographic	890	396

The radiation dose obtained at different distances from the camera when the door is open and closed is discussed in Table 2. This table also describes the radiation doses when the source is in the different positions. This illustrates the fact that, before working in front of the camera, the source should be in the storage position to minimize radiation dose. This also illustrates that personnel should never stand in front of the camera when the shutter is open.

2.2.1.5 Interlock System. An interlock system prevents personnel access to unsafe areas. It consists of a key switch on the control panel, personnel safety plug box at the access door, and safety switches connected to all access doors. If for any reason the chain is broken, the camera shutter will automatically close and cannot be reopened until the reason for closure is corrected.

2.2.2 Imaging System (IS-10)

The IS-10 consists of an image system carriage, cassette holder, and cassette. The system is pictured in Figure 9.

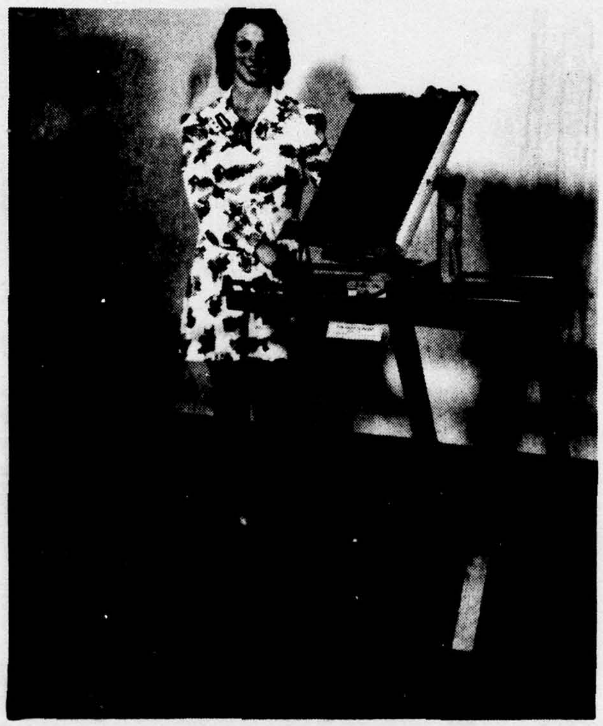

Figure 9. Imaging system (IS-10)

2.2.2.1 Image System Carriage. The image system carriage (Figure 9) is the mobile part of the system which can position the cassette holder at

a specified distance from the camera. The carriage is mounted on a track that is marked in 2-foot increments, representing the even integral distance of the carriage from the aperture. Once moved to the specified position the carriage can be locked by pushing a ball lock pin into the hole. This description of carriage movement applies to distances greater or equal to 4 feet (as marked on track). In the case of distances less than 4 feet, the carriage is positioned in a different manner.

To position the carriage closer than 4 feet, an interference problem with the door had to be resolved. This was accomplished with a nitrogen-actuated arm which automatically pulls the carriage to a position 31-1/8 inches from the collimator after the shutter is opened. Figure 10(a) illustrates the mechanism, while Figure 10(b) shows the carriage pulled under the shutter by the arm. In case of any break in the interlock chain, the arm automatically pushes the carriage away from the shutter before the shutter closes.

2.2.2.2 Cassette Holder. The cassette holder is mounted on a tubular track on the cassette holder carriage (Figure 9). It can be moved on these tracks to position the imaging plane at an exact distance on the carriage. These tracks make the cassette holder variable for another 28 inches after the carriage has been locked into place. This measurement added to the distance of the carriage is the exact distance of the imaging plane from the collimator.

The cassette holder can also be moved axially to the plane of the incoming neutron beam. This feature allows the sample (when mounted to the cassette holder) to be radiographed at any angle.

2.2.2.3 Cassette. Figure 11 illustrates the cassette and converter system. The cassette is composed of an aluminum front cover, base, and vacuum gauge. The cover and base, when vacuum-sealed, form an air- and light-tight case which protects the film from light exposure, and also assures that the film and screen are in complete contact. The vacuum gauge measures the vacuum level attained by the vacuum pump and indicates whether the cassette is properly sealed.

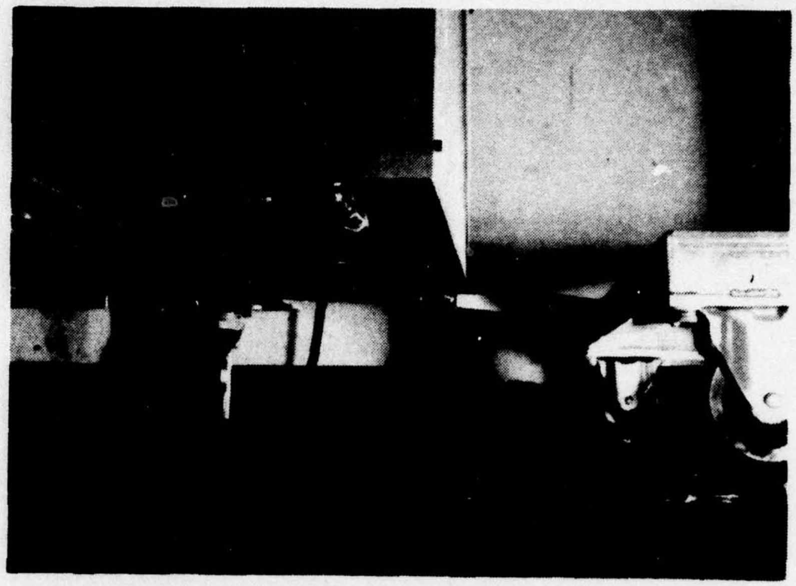

(a) automatic positioning arm

(b) carriage positioned by arm

Figure 10. Carriage positioning system

Figure 11. Cassette (from left to right) aluminum front cover, gadolinium screen, cassette base with vacuum gauge and nose connection

The converter system is a screen consisting of a 0.001-inch layer of vapor-deposited gadolinium covered by a coating of vapor-deposited sapphire, which protects the gadolinium from most types of moisture damage.

2.2.3 Beam Stop (BS-10)

The beam stop is a movable wall constructed of shielding materials to reduce the radiation dose from the neutron beam reaching the wall directly in the beam path.

The BS-10 was designed to reduce the radiation from the CFNR-10 system (when operating) to less than 50 mrem/hr on the exiting beam stop surface, the most extreme condition. This would be about three feet in front of the shutter (shutter open).

2.2.4 Control Panel

Figure 12 is a photograph showing the front of the CFNR-10 control panel. The controls illustrated are the power switch, shutter position switch, camera shutter key switch, and interlock chain. The lights above each switch indicate the operational mode of each control.

Front face

Figure 12. Control panel

2.3 SAMPLES RADIOGRAPHED AND INSPECTION RESULTS

The following samples were received:

a. Standard disks S_2 and S_3

b. Cracked samples C_1 and C_2

c. Doped* samples D_1 and D_2.

2.3.1 Standard Disks S_2 and S_3

2.3.1.1 Sample S_2. Figures 13 and 14 show the sample and physical layout of the holes. Table 3 lists these holes and their physical parameters. All of the holes were nominally 0.030 inch in diameter. Figure 15

*Metallic oxides with diameters $\leq$0.050 inch.

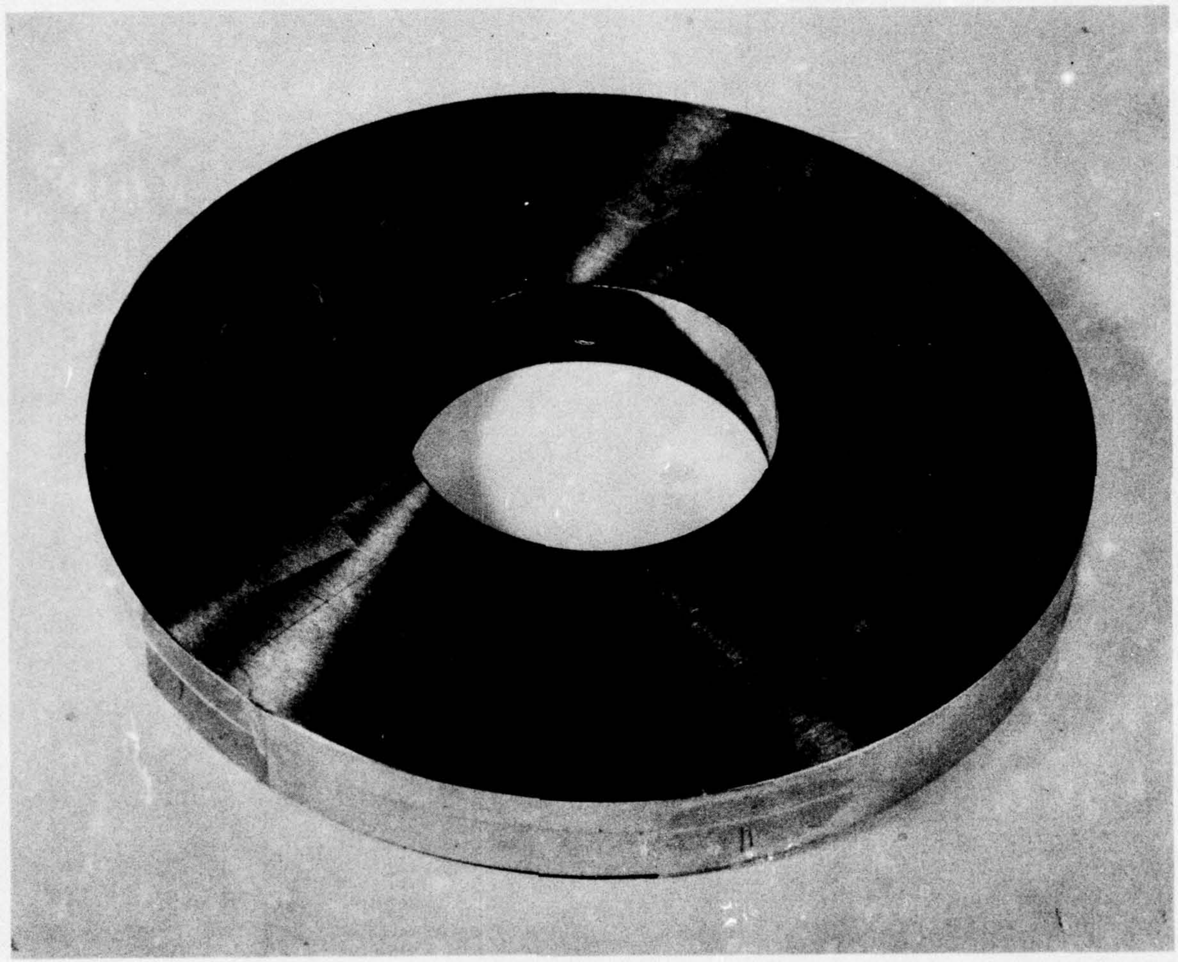

Figure 13. Sample S_2 - overall view showing hole locations. Each hole is covered with tape to prevent evaporation of penetrant solution.

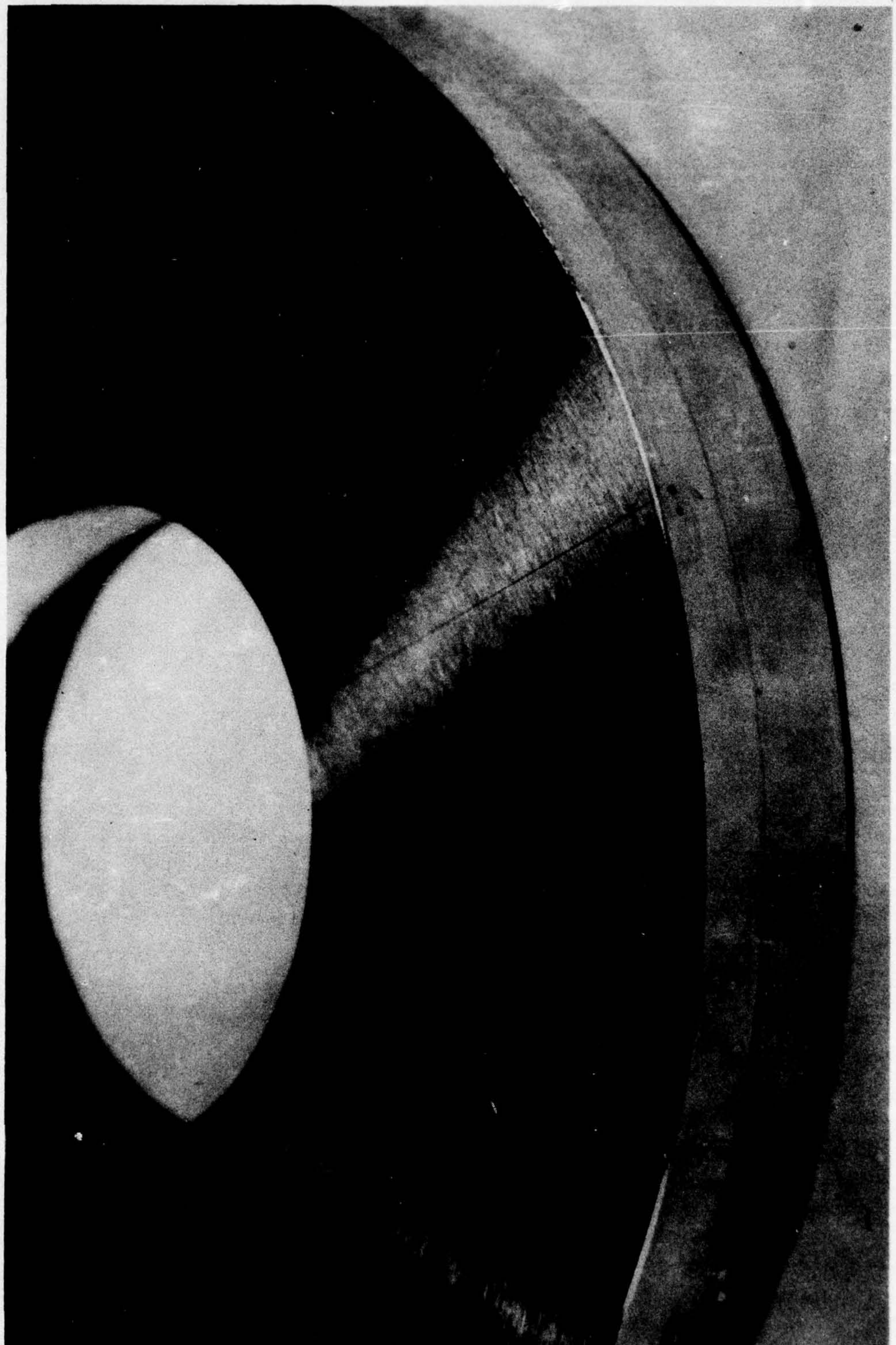

Figure 14. Sample S_2 - closeup view of hole 11 with tape removed

Table 3. Sample S_2 - Hole Locations

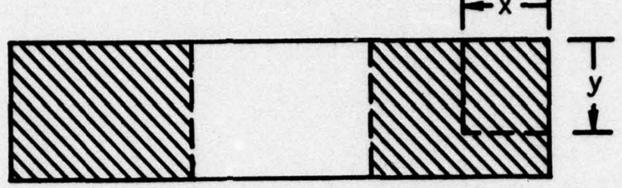

RT-12635

Hole	Depth[a] (mils)	x (mils)	y (mils)	Angle[b] (°)
1	500	--	579	(Ref.) 0
2	500	1012	-	30
3	500	--	491	60
4	400	1083	-	90
5	500	--	400	120
6	300	1100	-	150
7	500	--	310	180
8	200	1100	-	210
9	500/300	--	202	240
10	100	1115	-	270
11	500/100	--	110	300
12	600	1115	-	330

[a] Two depths indicate two holes at this location.

[b] When viewed from top of sample with hole location 1 as 0°, angles increase clockwise.

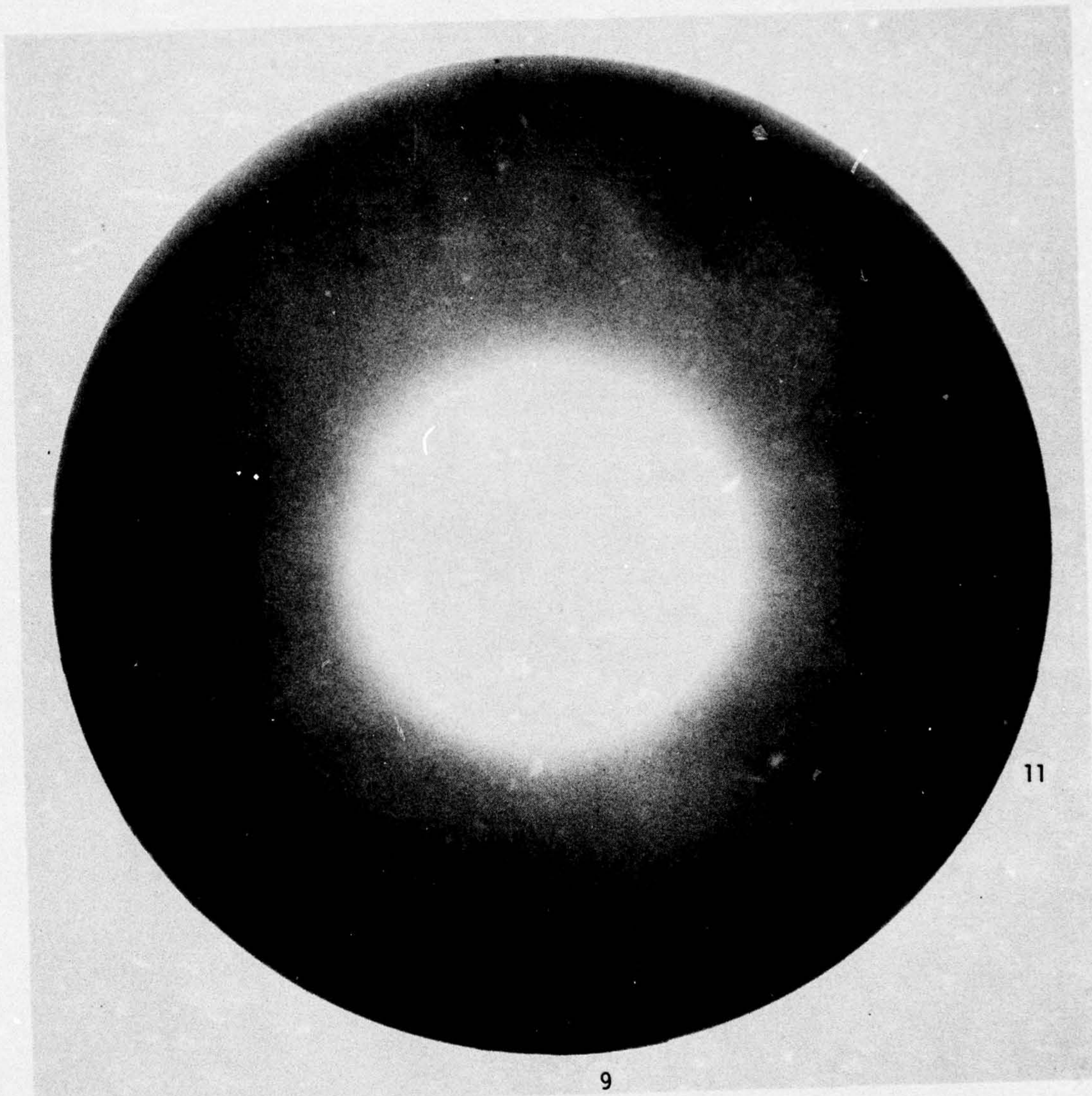

Figure 15. Neutron radiograph of sample S_2

is a positive copy of the n ray for this sample. Hole locations 9 and 10 are marked on this photo, and each have two holes. Due to the surface orientation with respect to the film, the hole numbers increase when going counterclockwise for this photo, opposite to the direction taken when viewing the sample from the top. For this radiograph the converter and film were placed on the upper surface, i.e., the surface containing the even-numbered holes, and the neutron beam impinged on the lower surface.

The shallow hole at location 9 is completely filled with penetrant, while the deeper hole has one small void. The shallow hole at location 11 is not filled, but is readily observable on the original radiograph. The deeper hole at this location is approximately two thirds filled, and again the unfilled portion is easily seen. One must remember that a copy of an original radiograph is not of the quality of the original. The remainder of the holes are all only partially filled to varying degrees, but in each instance the unfilled portion is discernable. One can also see the pieces of tape covering each hole location, used to prevent evaporation of the penetrant solution.

2.3.1.2 Sample S_3. This particular sample had a series of various sizes of holes on three different surfaces. Figures 16 and 17 show photos of the sample. Figure 18 shows the reference surfaces used, and the exact physical parameters are listed in Table 4. Figure 19 is a positive copy of the n ray for this sample and a section taken from a similar disk. As indicated in Table 4, hole sizes down to approximately 0.009 inch in diameter were observable on the *original* radiograph.

Owing to the fact that for this sample configuration the film and converter screen cannot be placed close to the surfaces containing the holes, several special cassettes were fabricated to minimize any geometric distortion.

One such cassette (flexible) consisted of the film and gadolinium converter sandwiched between two thin aluminum sheets sealed at the edges. This flexible cassette was then wrapped around a portion of the upper section shown in the diagram (see Figure 18) to encompass those holes measured

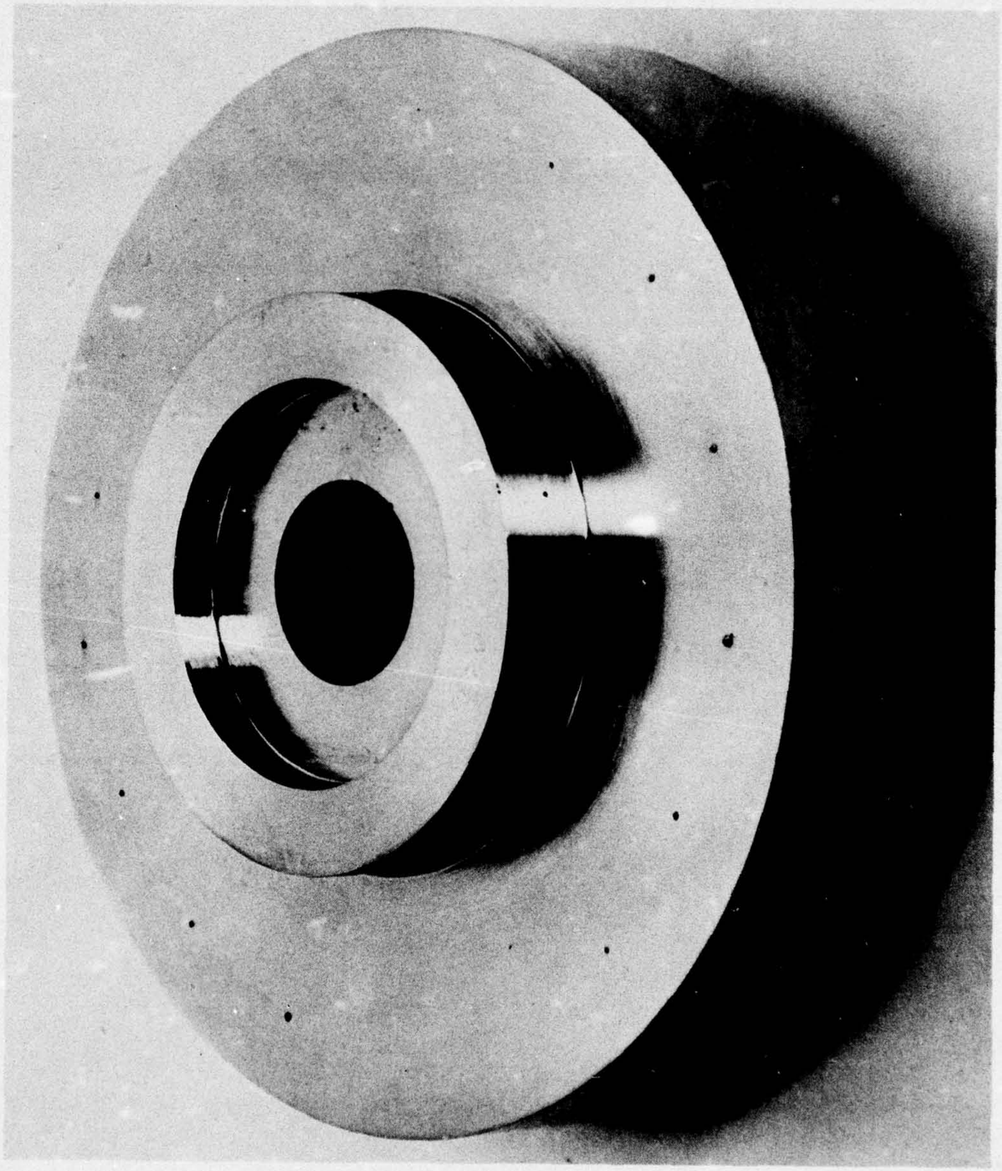

Figure 16. Sample S_3 - overall view showing the holes on the various surfaces

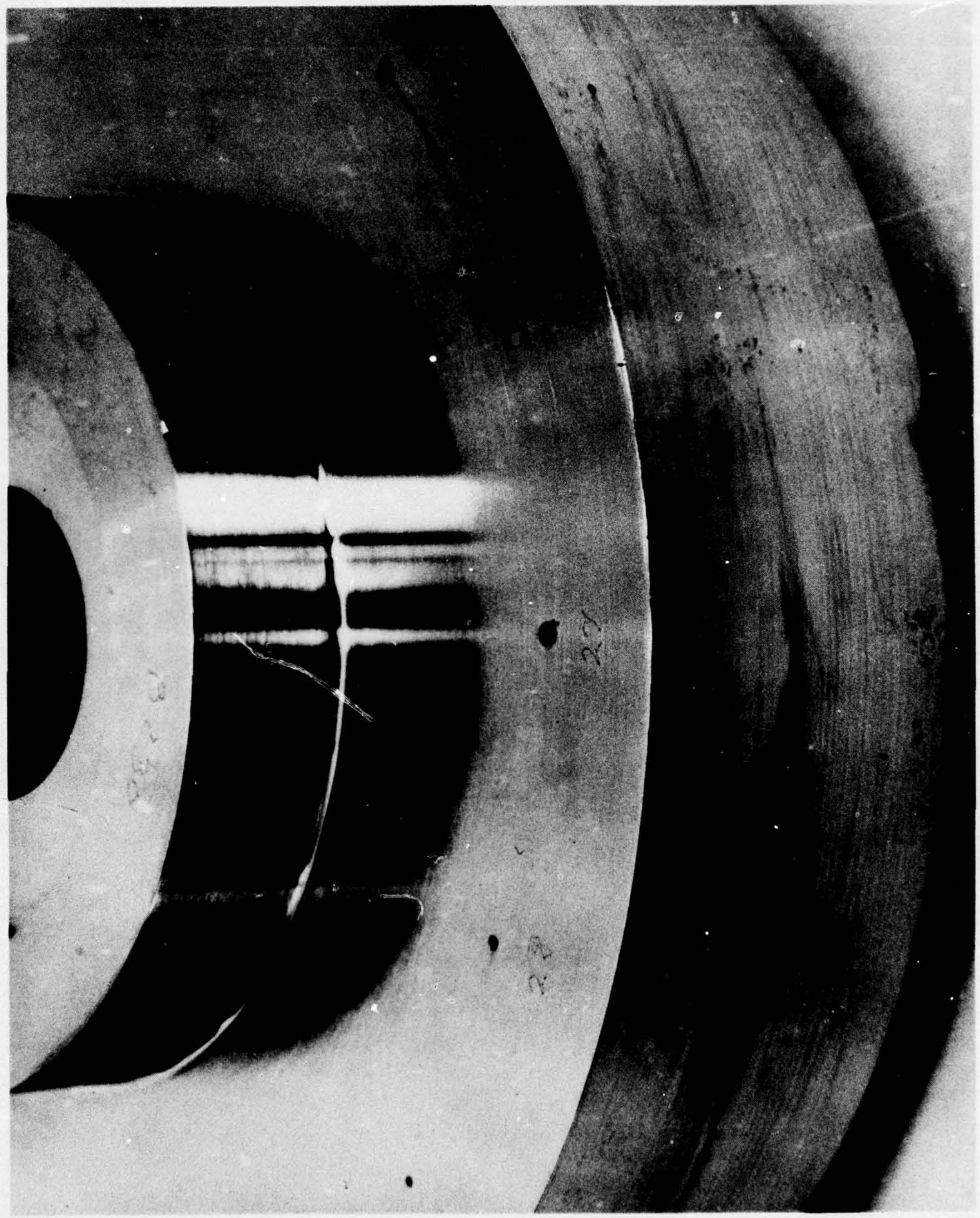

Figure 17. Sample S_3 - closeup view

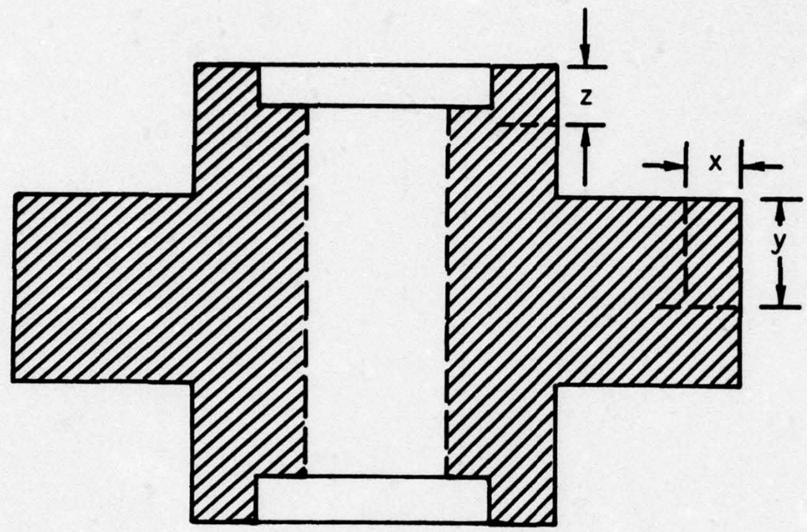

RT-12636

Figure 18. Sample S_3 - diagram showing distance measurements referred to the various surfaces

Table 4. Sample S_3 - Neutron Radiographic Record

Hole	Diameter (mils)	Depth (mils)	x (mils)	y (mils)	z (mils)	Angle (°)	Observable
1	31.5	500	-	165	- (Ref.)	0	Yes
2	31.5	500	-	260	-	17	Yes
3	31.5	500	-	375	-	39	Yes
4	32.3	500	-	500	-	60	Yes
5	31.5	500	-	620	-	78	Yes
6	47.3	100	490	-	-	5	Yes
7	32.3	300	490	-	-	27	Yes
8	33.3	500	470	-	-	49	Yes
9	33.3	700	405	-	-	70	Yes
10	31.5	890	508	-	-	90	Yes
11	31.5	∿25	-	-	150	45	No
12	31.5	50	-	-	150	78	No
13	12.3	∿15	435	-	-	109	No
14	11.4	125	420	-	-	130	No
15	9.6	75	420	-	-	153	No
16	9.6	100	465	-	-	173	No
17	26	200	485	-	-	198	Yes
18	10.5	90	-	200	-	100	Yes
19	10.5	90	-	275	-	121	Yes
20	8.8	90	-	450	-	141	Yes
21	12.3	90	-	512	-	163	Yes
22	12.3	165	-	615	-	185	Yes
23	10.5	100	-	-	255	142	No
24	12.3	100	-	-	310	173	No
25	18.4	100	475	-	-	219	Yes
26	20.1	290	475	-	-	242	Yes
27	20.1	375	475	-	-	264	Yes
28	∿35	∿20	540	-	-	286	Yes
29	19.3	500	490	-	-	306	Yes
30	19.3	500	-	110	-	209	Yes
31	20.1	500	-	250	-	231	Yes
32	16.6	550	-	340	-	251	Yes
33	19.3	500	-	515	-	276	Yes
34	21.9	500	-	635	-	296	Yes
35	21	∿40	-	-	339	241	No
36	22.8	50	-	-	277	274	No

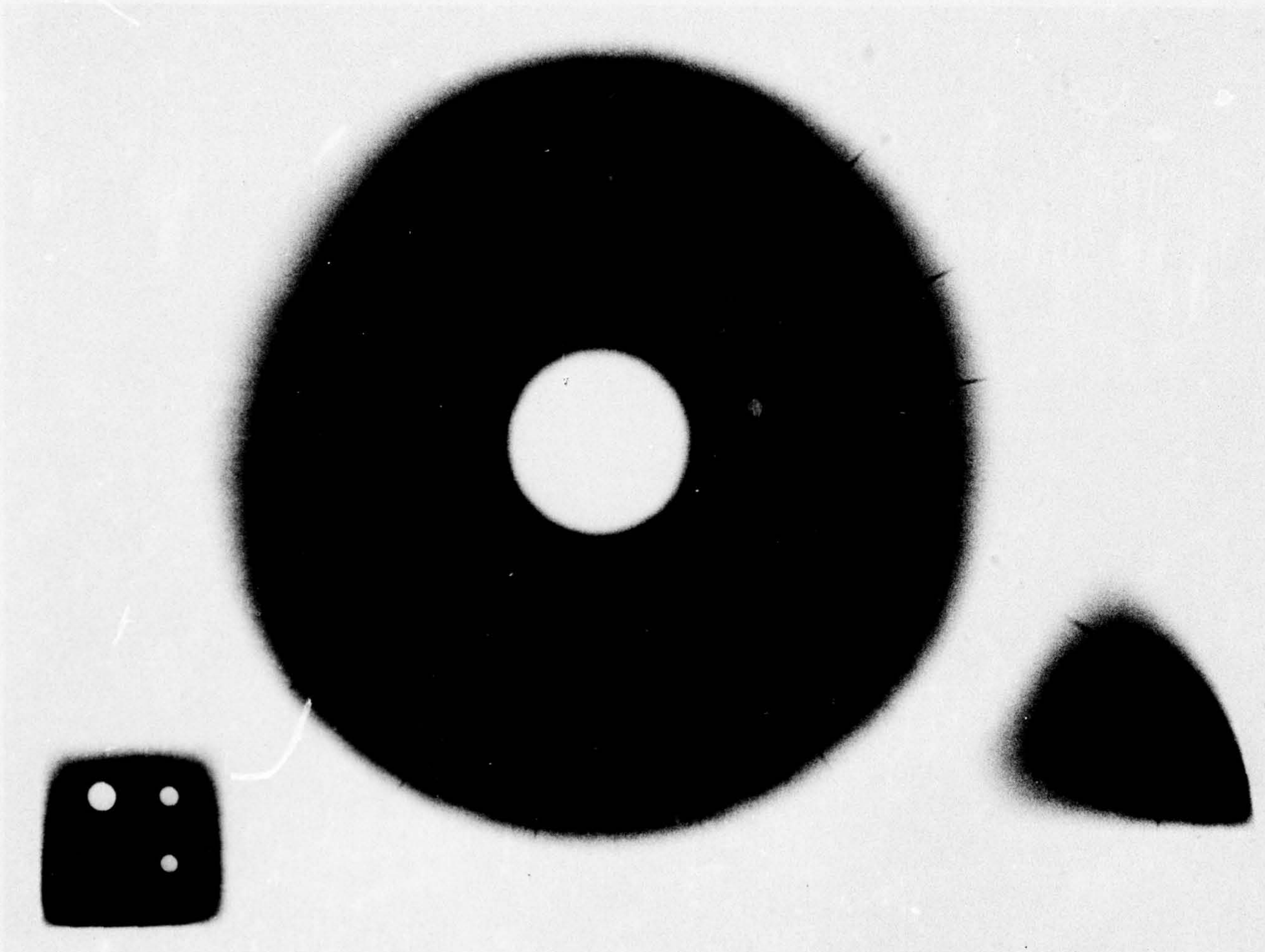

Figure 19. Neutron radiograph of sample S_3 and a test piece

in the z-direction. The sample was then oriented such that the impinging beam was at an acute angle with respect to the axis of rotation of the sample, whereby the neutron beam only passed through that portion of the sample containing the holes. The implementation of this technique was successful, even though a photographic interpretation is somewhat complicated by the unusual angle.

This flexible cassette was also used in the same configuration for taking an n ray by the transfer technique. For this, a thin foil of dysprosium and indium were used, wrapped in a polyethylene bag and then taped tightly against the upper section. The orientation is identical to the technique mentioned above, the only difference being that following the irradiation both foils were removed and sandwiched between two sheets of x-ray film and allowed to remain in a pressure cassette for several hours while the latent image on the foil was transferred to the film. After this, the film was developed in a normal way. The flexible cassette technique did not result in a significant improvement.

Another special cassette was fabricated that would fit flush against the upper surface containing those holes measured in the x-direction. The gadolinium converter and x-ray film were placed between two thin aluminum sheets. A hole was then cut in the center of this cassette that would allow the upper portion of the sample to protrude through (see Figure 18). The outer edges and inner hole of this cassette were then light sealed. This type of cassette does not allow intimate contact between the upper surface and the converter film to exist, thereby optimizing the photo resolution.

2.3.2 Cracked Samples C_1 and C_2

Sample C_1 is shown in Figure 20. One crack readily seen in the photo emanates from the indentation area and progresses over the upper surface approximately along the sample diameter. The maximum crack width, as examined with a microscope, seems to be on the order of 0.0005 inch or less. Sample C_2 is shown in Figure 21. There are two visually observed cracks in this sample, and both emanate from the left side of the sample

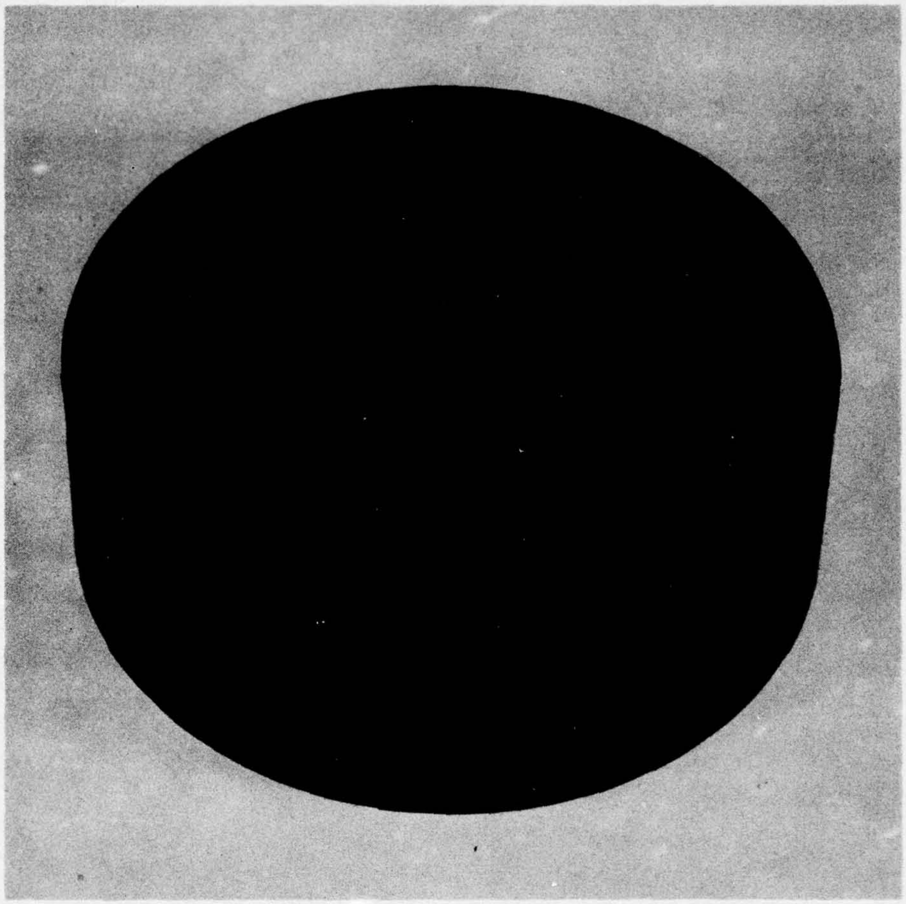

Figure 20. Sample C_1 - overall view

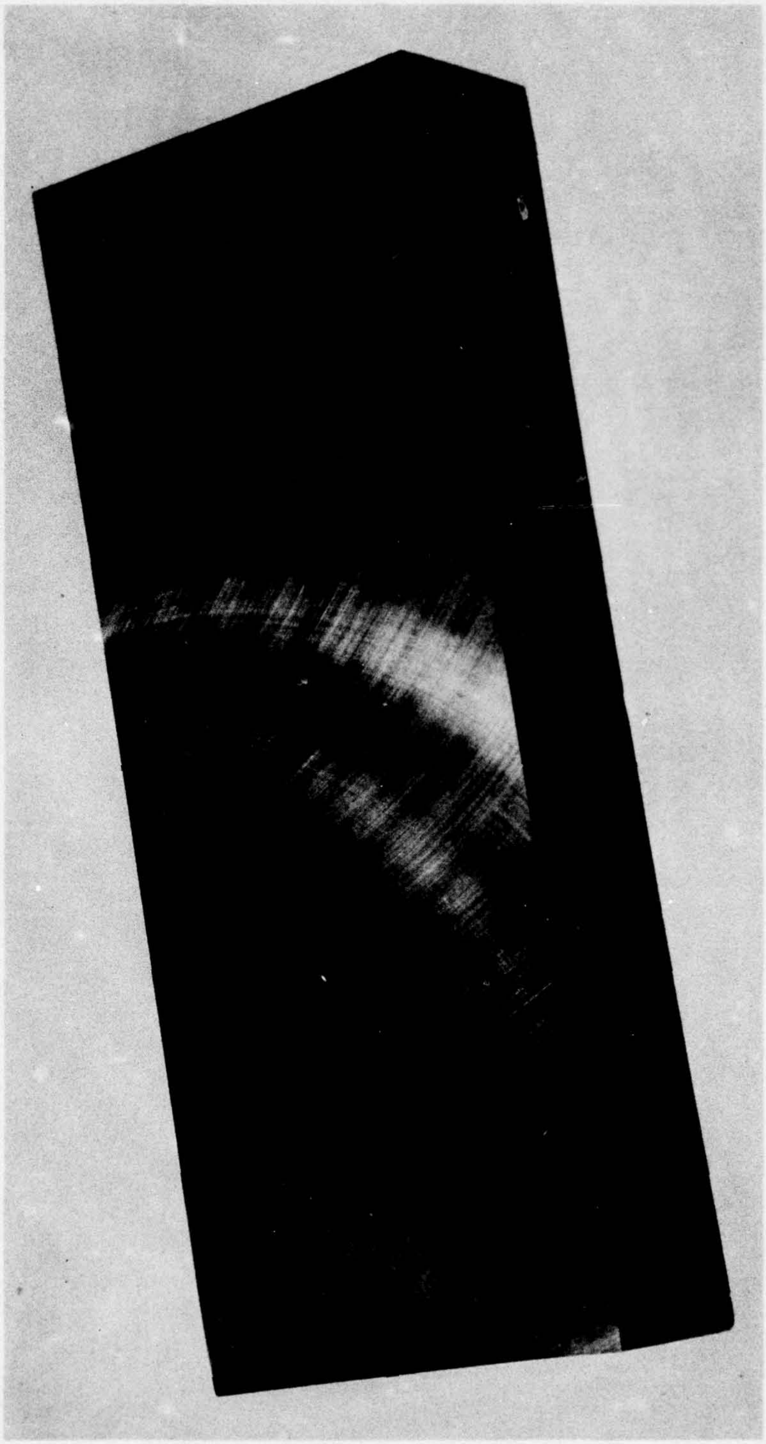

Figure 21. Sample C_2 - overall view

near the area where the triangular portion is removed. One crack is aproximately 1 cm in length, while the other forms an arch terminating near the upper left-hand corner of the sample.

These samples were also impregnated with the penetrant solution mentioned previously. Sample C_1 was vacuum impregnated, while sample C_2 was both vacuum impregnated and then heated to ensure maximum penetration. These samples were then oriented with respect to the impinging beam so as to discover if there is an optimum orientation for the beam. No radiographic evidence of the cracks was detected. As a means of comparison, an angular dependence using x rays was taken on sample C_1. There were no indications of cracks in any of the five orientations used.

2.3.3 Doped Samples D_1 and D_2

Preliminary inspection of these samples with the techniques used thus far indicated no areas with density changes outside the usual density gradients.

2.4 DISCUSSION OF RESULTS

2.4.1 Impact of Neutron Scattering on Resolution

Qualitative results of an n-ray radiograph were obtained utilizing visual inspection on a conventional x-ray viewing box. A trained observer can detect optical density changes on the order of 0.02 for a normal radiograph having an overall background density of 2.0. A scanning microdensitometer, Model MKIIIC manufactured by the Joyce Loebl Company in England, was used to obtain quantitative results from the areas of interest.

The minimum thickness of the penetrant that can be observed without scattering is calculated in the following example:

a. total macroscopic cross section, $\Sigma_T = 70\ cm^{-1}$ for $Gd(NO_3)_3 \cdot 6H_2O$ solution

b. optical density distribution from neutron component = 0.60. Again, we utilize the thermal-neutron attenuation relation

$$\frac{I}{I_0} = e^{-\Sigma_T t} \quad ,$$

where t is the thickness needed to obtain an optical density change of 0.02.

Substituting the above parameters, we get

$$t = \frac{1}{\Sigma} \ln \frac{I_0}{I} = \underline{0.0001} \text{ inch} \quad .$$

This thickness is indeed quite small, and is beyond the resolution limit of film and eye. However, the most important obstacle to overcome in the quest for very fine resolution is scattering of neutrons by the sample material, which to this point has been ignored. As seen previously for sample S_3, penetrant-filled holes down to diameters of 0.009 inch were seen, but the finer cracks in sample C_1 were not seen. Estimates of the maximum crack size were on the order of 0.0005 inch.

It is concluded that neutron scattering in the samples tends to reduce the fine resolution one might expect under ideal conditions.

2.4.2 Reduction of Scattering with a Post Object Collimator

In an attempt to overcome this problem, a post object collimator, placed between the sample and the film, was tried. This collimator consisted of an aluminum honeycomb structure with a thickness of one inch, with 0.1-inch cell spacings. Thus, the grid ratio (i.e., the thickness of the structure to its cell spacing) is ten. The collimator was dipped in a paint solution containing gadolinium. When dried, the gadolinium was evenly distributed over the walls. It effectively captures all thermal neutrons impinging on these surfaces. For the grid ratio of ten, those neutrons impinging on the surface of the collimator at angles greater than six degrees should be effectively eliminated from contributing to the radiograph due to absorption by the gadolinium.

Since sample S_3 had been sent to another group and was unavailable for testing the effectiveness of the post object collimator, a number of high-density polyethylene samples were prepared. They were one inch thick and contained various sizes of holes, ranging from 0.250 to 0.030 inch. Neutron radiographs were taken with and without the collimator. A comparison did not show any noticeable improvement. If the collimator did indeed improve resolution, the effect was offset by the fact that the stationary collimator grid was strongly imaged on the radiograph.

2.4.3 Summary of Results

As can be seen from the results with the direct exposure technique on samples S_2 and S_3, penetrant-filled holes with diameters down to 0.009 inch can be detected in the HIP material when the distance from the hole to the imaging system does not exceed approximately 5/8 inch. Scattering of the neutron beam in the sample is thought to be the primary factor limiting the defect resolution for this material. Experiments on material with similar high neutron scattering cross sections, utilizing a post object neutron collimator, did not conclusively show that the effect of scattering in a radiograph can be reduced with the collimator. However, the lack of improvement of resolution was probably due to deficiencies inherent in the utilization of a stationary grid collimator and could be overcome with an improved collimator design.

2.4.4 Recommendations

As a means of overcoming the grid overlay problem, a movable grid system was briefly investigated. The movable grid system was introduced after World War I for x-radiography, and is referred to as the Potter-Bucky grid, so called after the inventors. The grid system is moved during exposure in a random fashion. This is easy to attain for normal x-ray exposures, since the times here are generally on the order of seconds. However, for the long exposure times normally encountered in neutron radiography, a more elaborate system lasting for hours must be devised.

Design of a Potter-Bucky grid had barely begun when the decision was made to alter the technical direction for the remainder of the program and take a first, brief look at the feasibility of applying the recently developed IRT Photon Scattering Gauge.

3. PHOTON SCATTERING GAUGE INSPECTION

3.1 GENERAL

In connection with a comprehensive evaluation of NDT techniques potentially applicable to the flaw-inspection of HIP components to be used in the T-700 engine, IRT's newly developed photon scattering inspection technique was tested during the final stage of the program. IRT had only recently completed development and testing of a test bed for evaluation of the photon scattering inspection technique for the highly specialized case of high resolution flaw inspection in the explosive filler of 105-mm projectiles (Ref 13). The test program had just been concluded with a clear demonstration of the feasibility of the technique for rapid, automatic, filmless inspection of 105/155-mm projectiles.

Since the original test bed had been designed for a particular type of sample which is configured quite differently from the available HIP test samples, the existing gauge geometry had to be altered to accept the new samples. The resolution characteristics of the gauge, having also been designed to meet the inspection criteria applying to 105-mm shells, were not optimal for the inspection of HIP samples. A change, however, was considered to be outside the scope of the present evaluation effort since it would have entailed a major redesign of the basic radiometric system geometry. Instead, the measurements with the existing gauge are to demonstrate the capabilities of the technique within its present design limits. Use is subsequently made of a previously established parametric data base to project the performance of a system tailored to the needs of flaw inspection in HIP materials.

3.2 PHYSICAL PRINCIPLE

This radiometric technique is based on a simple physical principle. It is characterized by a three-dimensional, highly localized response that can fully identify type, size, and location of defects in the specimen with a high degree of resolution and sensitivity, even in the presence of severe defects in other parts of the specimen.

3.2.1 Basic Radiation Principle

The photon-scattering gauge utilizes the fact that gamma radiation interacts with the material which it passes through by scattering a portion of the incident beam away from the incident direction. This type of interaction, known as Compton scattering, is a well understood phenomenon. As photons exceed about 200 keV in energy, they almost exclusively interact with the electrons in the target material by transferring only part of their energy to the electron during a collision. Conservation laws require that the photon be deflected in a particular direction as a result of this collision. Energy loss and change in direction are unambiguously correlated. A small loss of energy is associated with a small angular deflection; increasing energy loss corresponds to increasing deflection, with maximum energy loss occurring when the photons are scattered through 180 degrees.

With increasing incident photon energy, a growing fraction of the scattered radiation falls in the forward direction, independent of target material, while the total probability for the occurrence of Compton scattering depends on incident photon energy and material characteristics. Generally, photons in the energy range of 200 to 1500 keV almost exclusively interact by Compton scattering with all but the heaviest elements. As the incident energy exceeds 500 keV, the number of scattered photons becomes practically independent of material composition and depends only on the mass of the scattering target. In other words, the number of photons scattered from a unit volume element in the target depends only on the amount of material in this volume element. We shall see that the number of scattered photons increases linearly with the amount of material in the target volume element.

A selected portion of the scattered radiation is usually measured by a radiation detector placed at a certain angle to the incident beam (see Figure 22). The detected scattered radiation results from Compton interactions in the volume element defined by the intersection of the incident

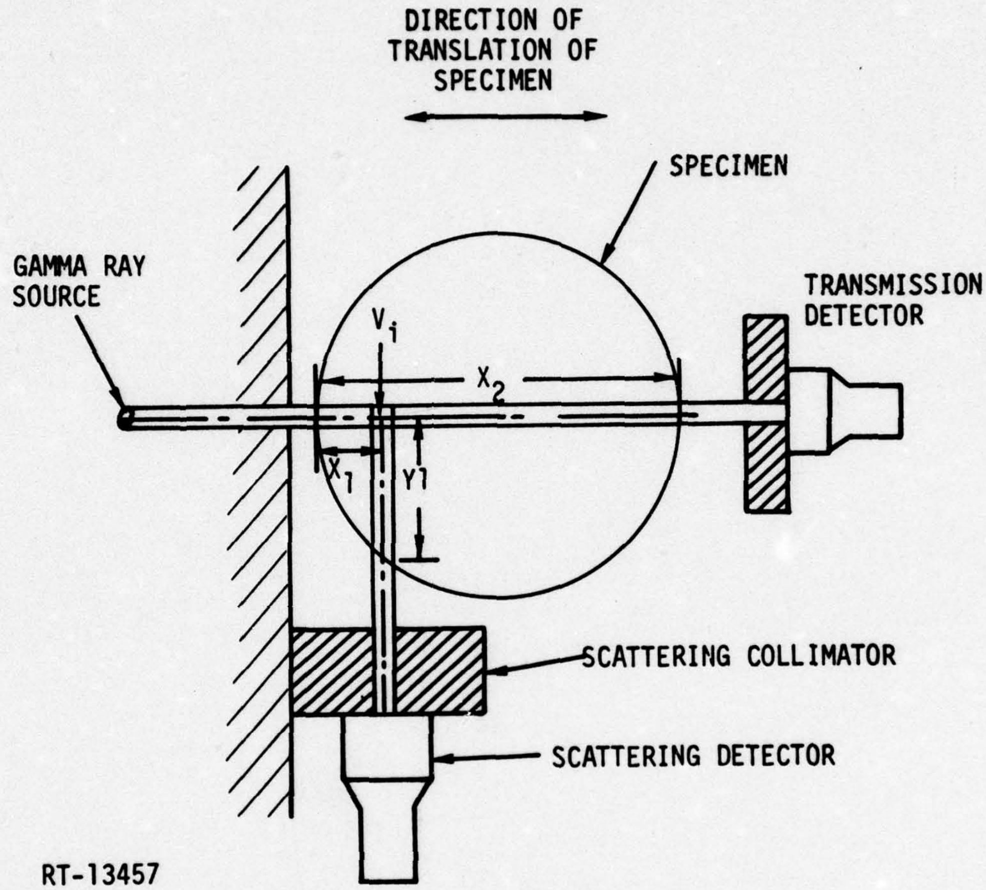

Figure 22. Schematic representation of a photon scattering gauge in comparison to a transmission gauge

beam and the detector collimation. Consequently, the volume element from which the scattered radiation originates appears to the detector like a source of radiation whose intensity depends on the amount of material contained in this inspection volume element. The introduction of a void into the volume element means a reduction in the amount of material available to

scatter gamma rays, and consequently results in a decrease in the detector response. On the other hand, the presence of an inclusion causes an increase in the detector response.

If the inspection volume element is selected sufficiently small so as to represent only a small fraction of the entire sample volume, the detector response becomes highly localized, and consequently is less subject to interference from signals from the rest of the sample. It also becomes highly sensitive to even minute voids as the void and inspection volume become comparable in size.

In the schematic representation of a photon-scattering inspection device shown in Figure 22, the specimen is positioned before the source collimator. A scattering detector with a suitable collimator views the sample from the side at a selected angle to the direction of the incident radiation. The 90-degree angle chosen for the schematic representation in Figure 22 is arbitrary, and does not imply that it is the optimum angle for a scattering gauge in general, or for this application in particular.

The Compton scattered radiation, which is measured by the scattering detector, originates in the volume element defined by the intersection of the collimated interrogating gamma-ray beam and the inspection aperture determined by the collimator in front of the detector.

3.2.2 Detector Response and Sensitivity

In order to understand the characteristics of the photon-scattering gauge in some detail, we shall now develop a general analytical formalism of radiometric techniques which allows a quantitative evaluation to be made. It is convenient to use the standard transmission technique as a point of comparison, since it is easily understood and forms the basis for the well-known radiographic method. In this elementary treatment, the secondary effects of small-angle scattering of the beam and of contributions from multiple scattering in material surrounding the beam are neglected.

3.2.2.1 Transmission Gauge. Referring to the arrangement in Figure 22, we can write the response of the transmission detector as follows:

$$R_T = I_o e^{-\mu\rho X_2} \tag{3.1}$$

where

I_o = incident gamma-ray flux from the source

$\mu\rho$ = total gamma-ray attenuation coefficient for the material of the specimen expressed for convenience as the product of the density (ρ) and the mass absorption coefficient (μ) with units cm^2/g

X_2 = material thickness as illustrated in Figure 22.

We are interested in knowing the sensitivity of the response R_T tc imperfections in the material represented by changes in X_2. These could, for example, consist of small voids which effectively cause decreases in this quantity. The fractional change of Eq. 3.1 can be expressed as

$$\frac{\delta R_T}{R_T} = -\mu\rho X_2(\delta X_2/X_2) \quad . \tag{3.2}$$

The left-hand side of this equation is the fractional change in the transmission response, and the right-hand side shows how this is related to changes in path length through the specimen.

That is, for a defect of width, W_d, in the material,

$$\frac{\delta_{RT}}{R_T} = -\mu\rho X_2 \frac{W_d}{X_2} \quad . \tag{3.3}$$

The most important generalization in the above analysis of the transmission response lies in the observation that the change in response is proportional to the ratio of the *size of the imperfection* to the *thickness* of the specimen for a given sample. We shall have an occasion to return to this concept after looking at the analysis of the photon-scattering technique for gauging.

3.2.2.2 Scattering Gauge. With the background provided by the previous discussion, we can proceed directly into an analysis of the photon-scattering gauge. Again referring to Figure 22, we can write the scattering response, R_s, by stepping through the sequence of interactions which occur. The scattering detector views a small volume at a position X_1 from the inner surface of the sample. Thus, for the assumed ideal conditions, the gamma rays which reach this point are given by

$$I = I_o e^{-\mu\rho X_1} \quad . \tag{3.4}$$

At the inspection point X_1, scattering events occur in the inspection volume, V_i, and those which scatter into the direction of the detector can be written as

$$I V_i \rho_i \mu_i \Delta\Omega f(\theta) \quad , \tag{3.5}$$

where I is from Eq. 3.4, $\Delta\Omega$ is the solid angle subtended by the detector at the scattering volume, and $f(\theta)$ is an angular distribution function which expresses the distribution of Compton-scattered photons. We use ρ_i and μ_i to represent the values of these parameters averaged over the inspection volume V_i.

The photons which scatter in the inspection volume and are degraded in energy according to the law of Compton scattering suffer an attenuation in reaching the detector, which is given by

$$e^{-\mu'\rho Y_1} \quad , \tag{3.6}$$

where the primed mass absorption coefficient indicates that the scattered gamma rays have a lower energy than the incident gamma rays. The overall scattering response is just the combination of the above three relations,

$$R_s = I_o V_i \rho_i \mu_i \Delta\Omega(\theta) \; e^{-\mu\rho X_1} \, e^{-\mu'\rho Y_1} \quad . \tag{3.7}$$

Now, following the same procedure as before to find the sensitivity of the scattering response to defects in the various parameters, we obtain the fractional response change

$$\frac{\delta R_s}{R_s} = \left(\frac{\delta\rho_i}{\rho_i}\right) + \left(\frac{\delta\mu_i}{\mu_i}\right) - \mu'\rho Y_1 \left(\frac{\delta Y_1}{Y_1}\right) - \mu\rho X_1 \left(\frac{\delta X_1}{X_1}\right) . \tag{3.8}$$

Equation 3.8 is the scattering analog of Eq. 3.2, and can be seen to have four terms which are similar to those of Eq. 3.2. These terms originate from the transmission processes which are part of the photon-scattering method, and affect the scattering response in the same manner as discussed above. In particular, their effect on the scattering response depends on the ratio of the defect size (δX_1 or δY_1) to the *path length through the material.* We shall concentrate our attention on the first two terms of Eq. 3.8, which express the effect of changes in average density and composition of the inspection volume V_i.

a. $(\delta\mu_i)/\mu_i$

This term refers specifically to changes in atomic composition of the inspection volume, the most common occurrence being an inclusion of some foreign substance. This term has a negligible effect on the scattering response for any inclusion with atomic number less than tin (Sn), and rises to an effect of about 10% for lead (Pb) for 1.0-MeV gamma rays.

b. $(\delta\rho_i)/\rho_i$

This term refers to density changes due either to voids or inclusions. In the case of inclusions, these will typically be lower in density than the surrounding material.

The most illuminating example of the photon-scattering technique is the case of a small defect. If the inspection volume is V_i and the defect volume is V_d, combining the effect of the first two terms in Eq. 3.8 gives the general result

$$\frac{\delta R_s}{R_s} = \frac{V_d}{V_i}\left(\frac{\mu_d \rho_d}{\mu \rho}\right) - 1 \quad . \tag{3.9}$$

In the special case of a small void in the material, we obtain

$$\left|\frac{\delta R_s}{R_s}\right| = \left|\frac{V_d}{V_i}\right| \quad , \tag{3.10}$$

which says that the fractional change in response is just equal to the ratio of the *defect volume* to the *inspection volume*. This is a very important result, since it provides a concise proof of the superiority of the sensitivity of the photon-scattering technique over the transmission technique. Simply stated, since the change in the transmission response is proportional to the ratio of the defect size to the total thickness of the specimen (i.e., Eq. 3.3), the above result shows that the scattering technique is *more sensitive* than the transmission technique by a factor approximately equal to the ratio of the *size thickness of the spectrum* to the *length of the inspection volume* V_i. This can be a very large factor indeed.

3.2.3 Conceptual Description of Technique Implementation

Conceptually, a complete scan of the specimen is accomplished by rotating it about an appropriate axis, translating it along a line parallel to the interrogating beam such that the scattering detector scans it from wall to center, and moving it up or down. The volume inspected during one revolution is an annular ring (preferably concentric with the center of the sample) with a cross-sectional area equal to that of the inspection volume element. The data are recorded as the number of gamma rays which are scattered into the detector from each inspection volume element in this annular ring, along with the three-dimensional information defining the location of that inspection volume element, *viz.*, the angular location of the volume element, its radial distance from the center, and its vertical distance from a reference point at the base of the sample.

After one complete revolution, the specimen is moved horizontally by a discrete amount, depending on the size of the inspection volume element, and the process is repeated to scan another annular region at a different radius. The specimen is stepped in incremental amounts with each revolution, until the entire distance from surface to center has been traversed. At this point, the inspection of a thin disc whose thickness corresponds to the height of the inspection volume element is complete, and data from every volume element making up this slice is recorded, along with the three-dimensional position information. Next, the sample is moved vertically by an amount corresponding to the height of the inspection volume element, and inspection of the adjacent disc begins.

The three-dimensional data array is subsequently analyzed for variations in the number of counts per data point that may indicate statistically

meaningful deviations of material density as a result of defects. These deviations are then quantitatively analyzed for their magnitude, and correlated with statistically significant deviations in neighboring data points to define the size, shape, and orientation of the defects.

The photon-scattering gauge is thus seen to be an inspection device which provides a high-resolution, three-dimensional scan profile of the entire specimen. It performs a differential measurement which, with an appropriately small inspection volume element, not only identifies the presence of discontinuities (such as voids, cracks, and inclusions), but also provides data about their size, three-dimensional location, and orientation.

3.3 EXPERIMENTAL ARRANGEMENT

IRT assembled a conceptual model of the scattering gauge to demonstrate the capability of the photon-scattering technique.

As is shown in a schematic representation in Figure 23, it consists of four major subassemblies: the ^{60}Co isotopic source with shield and collimator, the photon-scattering detector with associated shield and collimator, the associated electronic data acquisition instrumentation, and the mechanical scanning device allowing inspection of the specimen.

3.3.1 Isotopic Source Assembly

^{60}Co is an isotopic source widely utilized in industrial and medical applications as a gamma-ray emitter because of a number of favorable characteristics. Every disintegration results in the emission of two energetic gamma rays, at 1170 and 1332 keV. Its half-life is relatively

long at 5.24 years, resulting in a theoretical specific activity 818 Ci/g. High intensity teletherapy sources with specific activities of up to 400 Ci/g are commercially available.

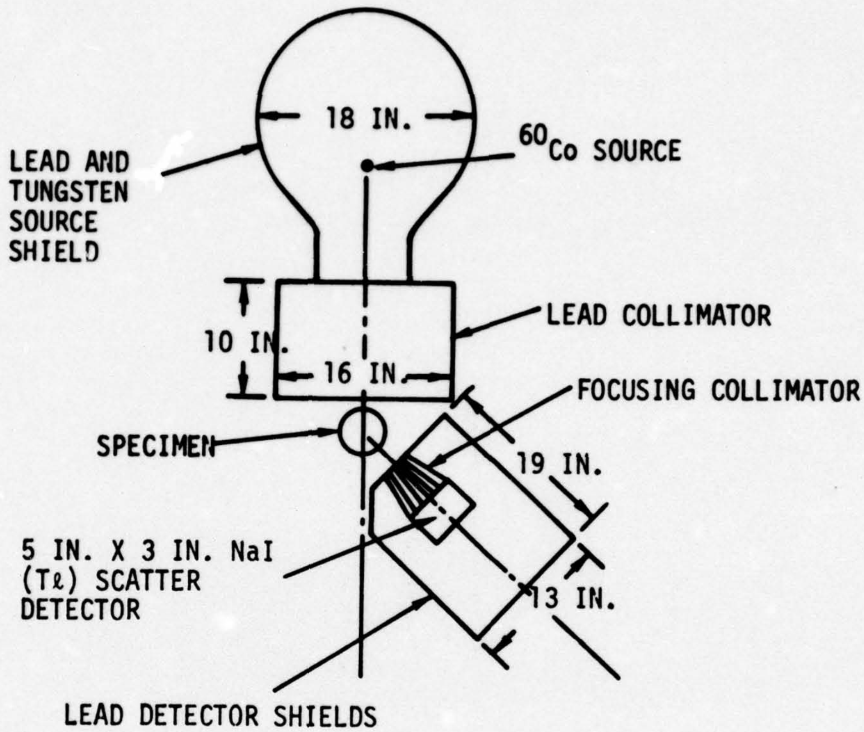

Figure 23. Schematic representation of geometrical arrangement of the photon-scattering test gauge

---

3.3.2 Source Collimation

The collimation necessary to define a small inspection volume element with a beam of small cross-sectional extent is provided by a 10-inch-thick lead collimator placed directly in front of the irradiator. At the center a single circular collimator hole with a 0.9-degree taper ranges in diameter size from 0.451 inch at the face nearest to the source to 0.134 inch at the opposite face. Geometrically speaking, and not considering the fact that the energetic ^{60}Co gamma rays penetrate to some degree through the wall of the collimator hole, this configuration defines circular umbral and effective penumbral regions with maximum diameters of 0.063 and 0.156 inch, respectively, at a point 2.5 inches from the face of the collimator. The diameter of the effective penumbral region is defined as the full width at half maximum (FWHM) of the penumbral cross section, as shown in Figure 24.

3.3.3 Photon-Scattering Detector

The photon-scattering detector consists of a NaI(Tℓ) scintillation detector, a collimator, and a cylindrical lead shield, as shown in Figure 25. All components are arranged axial to the axis of the detector. The axis of the detector assembly is placed at a 45-degree angle relative to the direction of the source beam.

3.3.3.1 NaI(Tℓ) Scintillation Detector. A 5-inch-diameter by 3-inch-thick NaI(Tℓ) scintillator with photomultiplier tube and tube base mounted in one integral assembly was selected, with the objective of combining good efficiency for the detection of energetic gamma rays scattered from the gamma-ray beam with as large a solid angle as possible for the interception

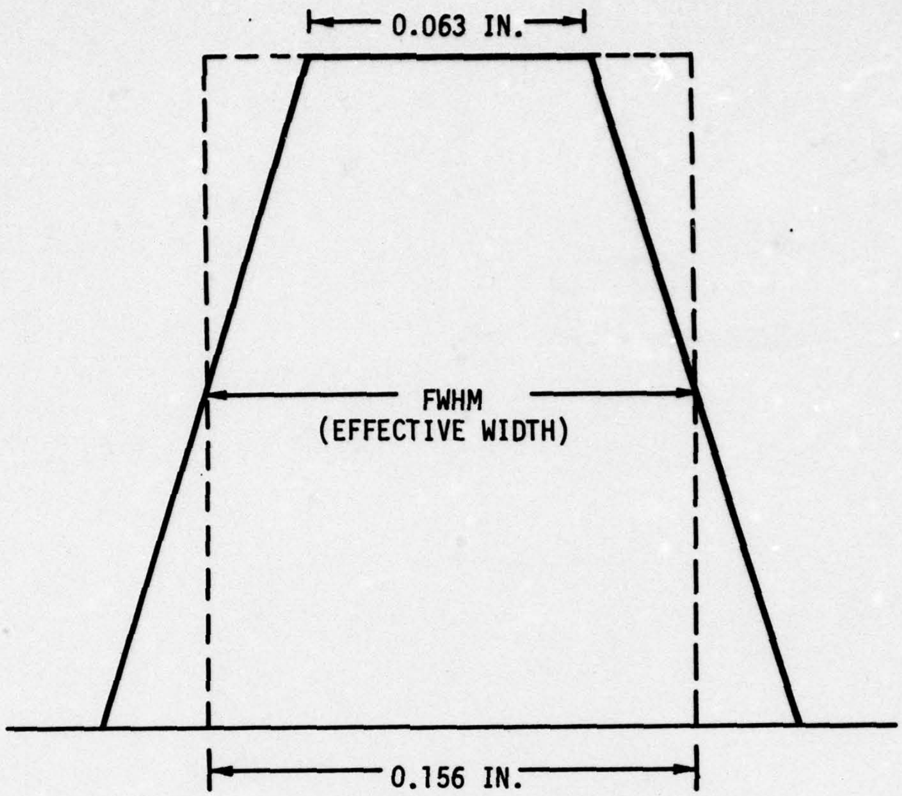

RT-13011

Figure 24. Effective width of the circular beam from the ^{60}Co source collimator

---

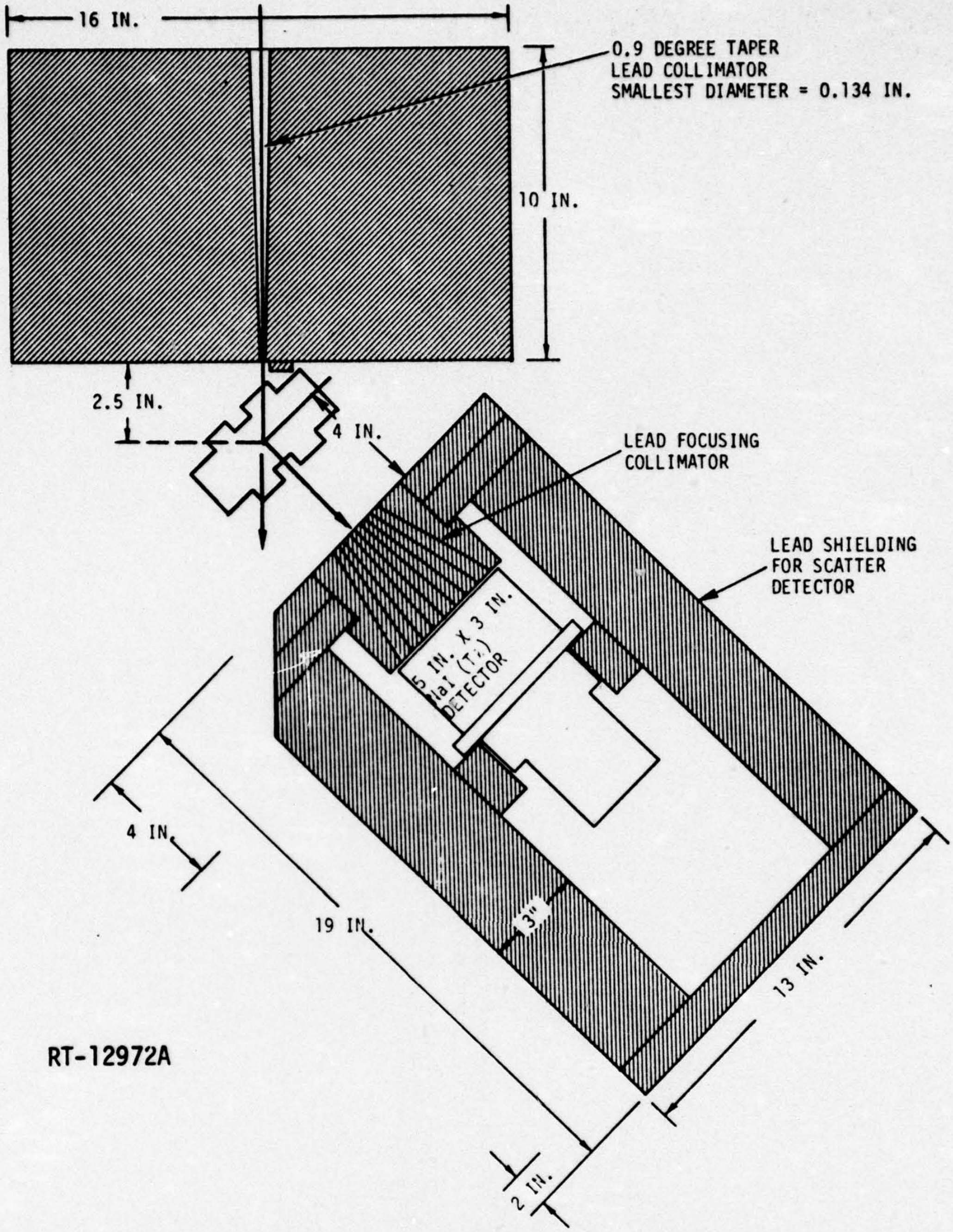

Figure 25. Schematic representation of the scattering detector in relation to the sample and ^{60}Co source collimator

of scattered radiation. It was the largest, most efficient scintillator available at the laboratory for this experiment. The detector is held in place inside the shield with concentric lead rings; its axis intercepts that at the gamma-ray beam at a point eight inches from its front surface, and 2.5 inches from the face of the source collimator.

3.3.3.2 Focusing Collimator. In order to take good advantage of the relatively large diameter of the photon-scattering detector while simultaneously maintaining the necessary resolution provided by a small inspection volume element, a special focusing collimator was designed.

The resulting collimator, fabricated at IRT for use in the conceptual model, is a 4-inch-long lead cylinder (exact length after machining of front end is 3-31/32 inches) with a concentric array of 217 holes angled such that their straight line extensions all converge to a point four inches from the face of the collimator (see Figure 25); hence, the name "focusing collimator." This focal point falls on the gamma-ray beam with which it defines the inspection volume element. In a cross-sectional view, the holes are arranged in a hexagonal pattern, i.e., each hole, except those at the periphery, has six neighbors. This constitutes the optimum pattern for arranging the largest number of holes in a given area consistent with the biggest possible separation between the holes.

All holes have a straight bore with 1/16-inch diameter. The distance between the centers of neighboring holes at the detector end is 0.29 inch, which leaves a minimum of 0.23-inch material between neighboring holes. At the opposite end, toward the inspection volume element, the distance between neighboring holes is reduced by 50% due to the ratio of 4 versus 8

inches for the distance from the face of the collimator to the focal point versus that from the face of the scintillator. This leaves a minimum of about 0.08 inch of material between neighboring holes. This minimum distance between holes could have been safely reduced by 50% without significantly degrading the resolution capability of the collimator, due to the fact that gamma rays scattering between holes are effectively absorbed in the collimator over its total length of four inches.

A 50% decrease in the distance between holes would result in an increase in the number of holes and, consequently, in the effective solid angle of the detector, of approximately a factor of four. However, the resulting, significantly improved efficiency of the photon-scattering detector was sacrificed to the convenience of fabricating the collimator. It was made by casting molten lead into a mold in which the holes were defined by 1/16-inch-diameter stainless steel welding rods held in place by commercially available plates with hexagonal hole patterns with 1/16-inch-diameter holes. The ratio of 2 to 1 for the hole spacings in the two ends was implemented by filling every hole in the plate nearest the focal point, and every other hole in the other plate. The hole spacing was thus dictated by the commercially available hexagonal hole patterns with the tightest packing of 1/16-inch-diameter holes. The selected choice in this case was a metallic loudspeaker grille.

The function of the focusing collimator is to direct to the detector the largest possible fraction of scattered radiation, consistent with its size, originating from material at the focal point, and to exclude radiation scattered from material surrounding the focal point. In other words, the collimator must be able to resolve the radiation from a certain volume

---

at the focal point from all other radiation. An estimate of the collimator resolution in the plane perpendicular to the axis on the basis of purely geometric considerations leads to an effective width of 1/8 inch, with a width of 1/16 inch for the umbra, and of 1/8 inch for the total extent of the penumbra at half maximum. These geometric considerations are strictly valid only for the center hole. They are somewhat modified by the superposition of all 217 holes.

The resolution characteristics were experimentally investigated by moving an isotopic gamma-ray source parallel to the front face of the collimator through the collimator axis and recording the detected radiation intensity. The measurements were recorded at several different distances from the collimator, including the focal distance of four inches. Ideally, for these measurements, a point source should have been used. Since no point source with sufficient intensity was available, a thin disc-shaped ^{137}Cs source, consisting of a thin deposition of isotopic material between two Mylar films, was used instead. The diameter of the source region is approximately 1/4 inch. To simulate a point source, it was positioned with its edge facing the detector. The resulting effective source width was approximately 0.002 inch.

The energy of 662 keV of the gamma rays emitted by ^{137}Cs is a fair representation of the energy interval of the scattered gamma rays, which ranges from 540 to 977 keV, with the majority of the gamma rays clustered around the 728-keV energy of the gamma rays scattered at 45 degrees.

The result of one resolution measurement at the focal point is shown in Figure 26. The results of this measurement are representative of the resolution properties for any direction in the plane perpendicular to the

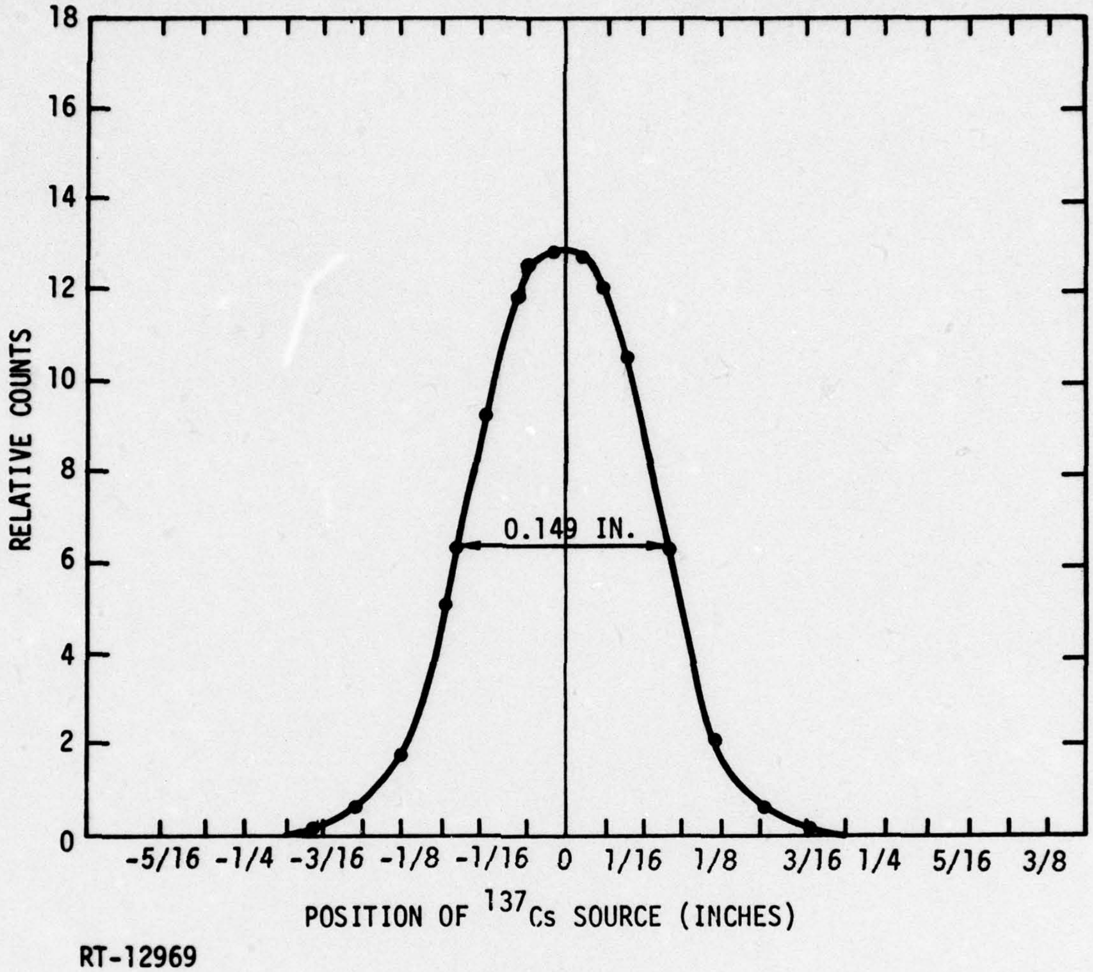

Figure 26. Experimental data showing the resolution of the focusing collimator in the plane perpendicular to the collimator axis. The data was taken at the focal point.

---

collimator axis due to the axial symmetry of this collimator. The value for FWHM of 0.149 inch is in good agreement with the theoretical prediction of 0.125 inch on the basis of purely geometric considerations for the center hole alone, under the exclusion of the effect of wall penetration of the gamma rays. Another factor likely to slightly degrade the measured FWHM to some extent is the fact that the ^{137}Cs source has a 0.25-inch extension along the axis of the collimator, with the result that some of the source material is positioned at a maximum distance of 1/8 inch from either side of the focal point. The measured resolution curve shows a flattening at the top roughly corresponding in width to the 1/16-inch diameter of the hole. Because of the axial symmetry of the detector, the length along the source beam of the inspection volume element, as well as its height, should be approximately 0.150 inch.

The effective resolution width of the collimator was more accurately determined to be 0.125 inch by placing thin steel rods into the inspection volume element. The effective beam width was determined to also be 0.125 inch. A calculation of the volume defined by the intersection of two cylinders with a diameter of 0.125 inch yields a value of 0.002 cubic inch for the inspection volume element.

3.3.4 Data Acquisition Electronics

As shown in Figure 27, the signals from the photon-scattering detector were amplified before they were energy analyzed by a single-channel discriminator. The discriminator output is counted in a scaler.

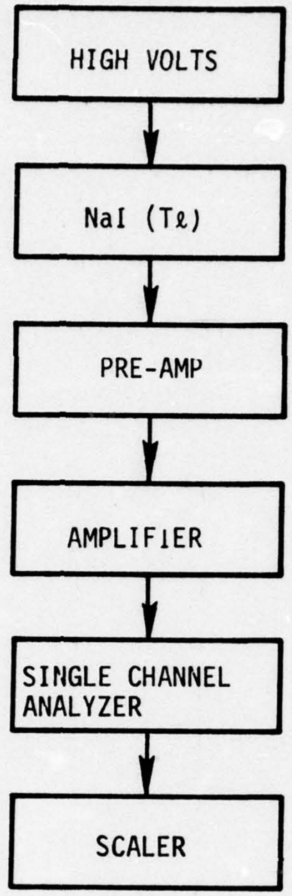

RT-12974A

Figure 27. Block diagram of the electronics for the conceptual model

3.3.5 Sample Scanning Device

The function of the sample scanning device is the precise and accurately reproducible locating of the sample at the focal point of the scattering detector, and to provide for three-dimensional adjustability in a manner that permits the focal point to be located anywhere within the sample. These holding requirements were implemented by mounting a sample fixture on a support frame which is attached to a platform by means of a manually operated screw drive assembly for horizontally moving the fixture support frame along the direction of the source beam. The platform in turn is equipped with three sets of linear bushings, permitting accurately controlled vertical movement along three vertical guide rods. The vertical positioning is affected by manual operation of another screw drive. Structural integrity of the system is provided by a support frame which is anchored against an adjacent wall to ensure structural rigidity of the assembly. Metallic rulers with engraved precision scales graduated in 1/64-inch steps are attached to the vertical support frame and to the vertically moving platform to permit reproducible vertical and horizontal adjustment of the sample holder to within 1/128 inch.

The sample holding fixture consisted of an aluminum saddle which held the sample in a vertical position. It supported the sample along its circumference from the bottom through a contact area extending for approximately 90 degrees. The contact area was carefully machined to match the sample S_3 radius. Short ridges on both sides of the contact area provided positive lateral positioning of the sample. A scale graduated in 1/16-inch steps was attached to the fixture on a radius identical to that of sample S_3. Thus, the sample could be rotated resting on its side without

displacing it horizontally or vertically. A fixture holding the sample on a shaft through the center would have been greatly preferred; however, sample size and gauge geometry did not permit such an arrangement without a major reconfiguration of the gauge, which would have been outside the scope of this preliminary feasibility study.

3.4 INSPECTION MEASUREMENTS

3.4.1 Sample

A total of 12 holes were inspected in sample S_3. The holes were 1, 5, 6, 10, 12, 14, 17, 26, 29, 30, 32, and 36. (Consult Table 4 and Figure 18 for exact locations of the holes.)

3.4.2 Inspection Procedures

The response to each hole was measured by following the same basic sequence of steps. First, the sample was placed on its side on the saddle-shaped holding fixture discribed earlier. Secondly, a determination was made of a suitable angle of the sample relative to the radiation beam. Thirdly, the horizontal and vertical positions of the sample relative to the beam and focal point were selected such that the focal point fell directly at the location of the hole. Finally, five one-minute counting periods were conducted at this location, as well as at locations to the left and right of the hole, rotating the sample on its stand. Typically, the stepwise rotational motion was performed in steps registering 1/8 inch on the circumference of the sample.

This process was rather time consuming, since it frequently involved several trial runs to find a reasonably suitable sample orientation for the inspection of a particular hole. This somewhat cumbersome procedure was necessary only because the geometry of the existing photon scattering gauge, which had been tailored for a different inspection task, did not provide for efficient placement and inspection of the sample which would have required placing the sample either horizontally or vertically on a motor-driven shaft to permit a more automated scan procedure than the one

improvised for this study. As it was, the scanning operation had to be completely conducted by hand with the experimenter manually setting the sample for each data point.

As a result of time limitations, not all holes could be scanned with the same thorough pre-scan positioning preparations. Instead, special attention was paid to holes 5 and 10. While a series of three measurements for hole 5 was made to demonstrate how the technique provides unambiguous data about the size of a hole, a special effort was expended on hole 10 to place the sample relative to the beam in such a way that the focal point truly fell on the defect as the sample was scanned, thereby maximizing the response. Therefore, only hole 10 can be used for quantitative statements about the resolution capabilities of the system. The remaining measurements primarily serve to demonstrate that defects are discernible over the range of different sizes and locations. In fact, only one hole (36) could not be inspected because there was insufficient room to position the sample in such a way that the focal point and hole 36 coincided.

It should be noted that any of these positioning considerations only apply in this special case of a feasibility study with equipment designed to address only the basic measurement parameters and not any operational aspects. Importantly, in a gauge designed for routine inspection of certain components, a motorized scan control system would conduct a full scan sequence, automatically positioning every volume element of the sample to the inspection point. There would be no need for searching for the best orientation of defining the presence of a defect with the least number of data points, as was the case in this study. The complete data set would automatically contain complete information, within system resolution limits, about any defect in the part.

3.4.3 Inspection Results

The inspection results are shown in Figures 28 through 31. For each hole, the response is displayed as the average number of counts per minute from the total of five one-minute runs, as a function of the position of

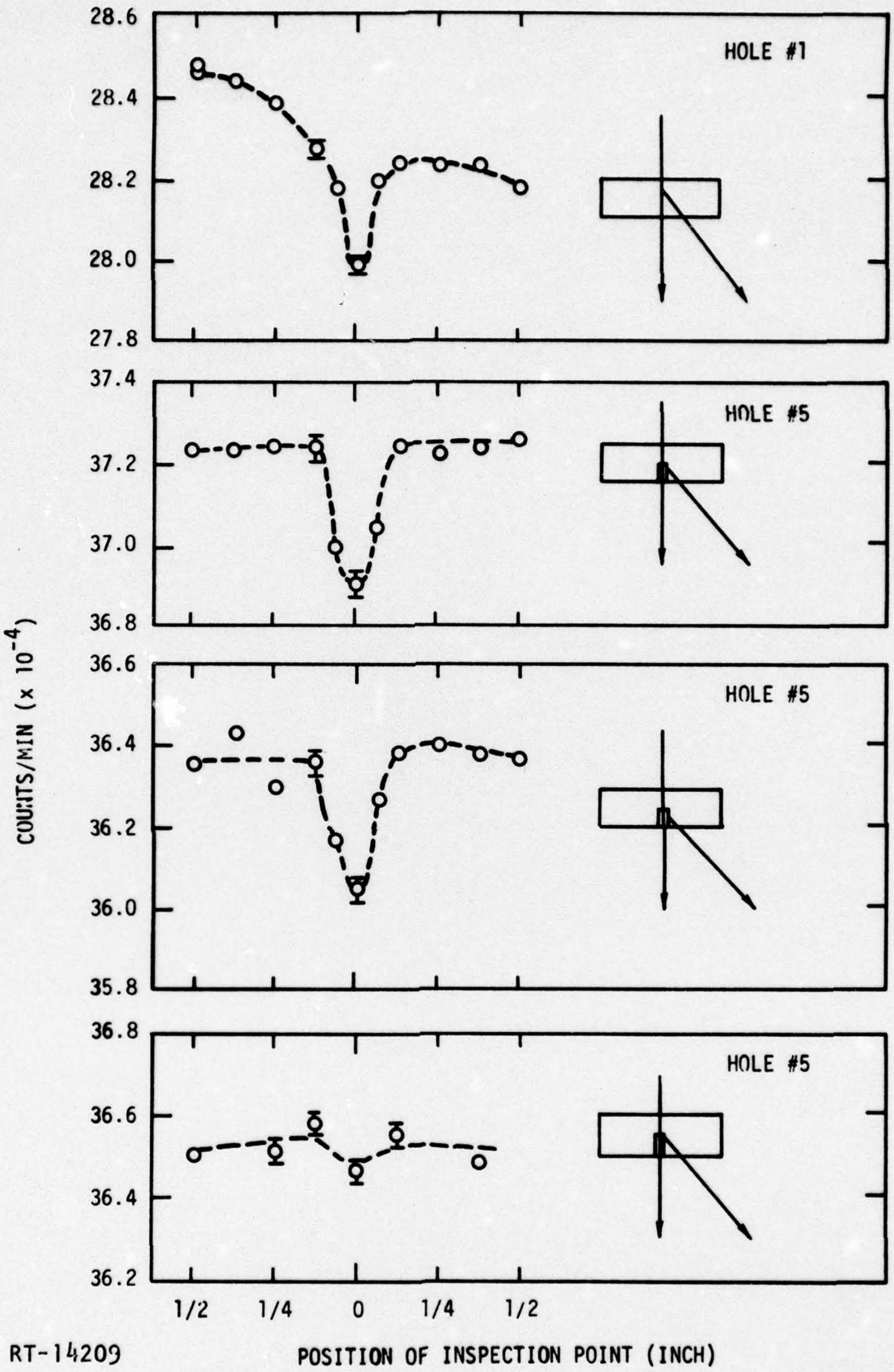

Figure 28. Response of the photon scattering gauge to hole 1 at one depth and to hole 5 at three different depths

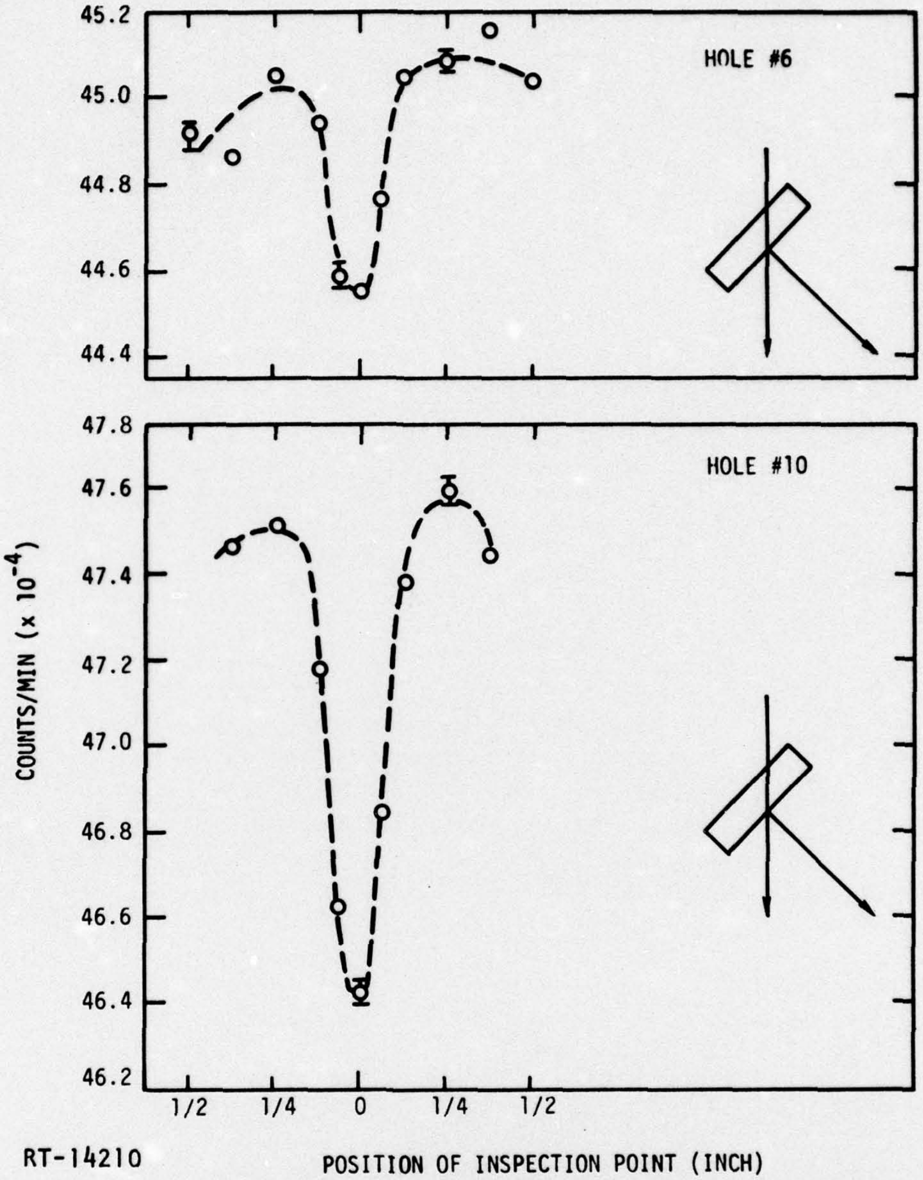

RT-14210

Figure 29. Response of the photon scattering gauge to holes 6 and 10 at one depth each

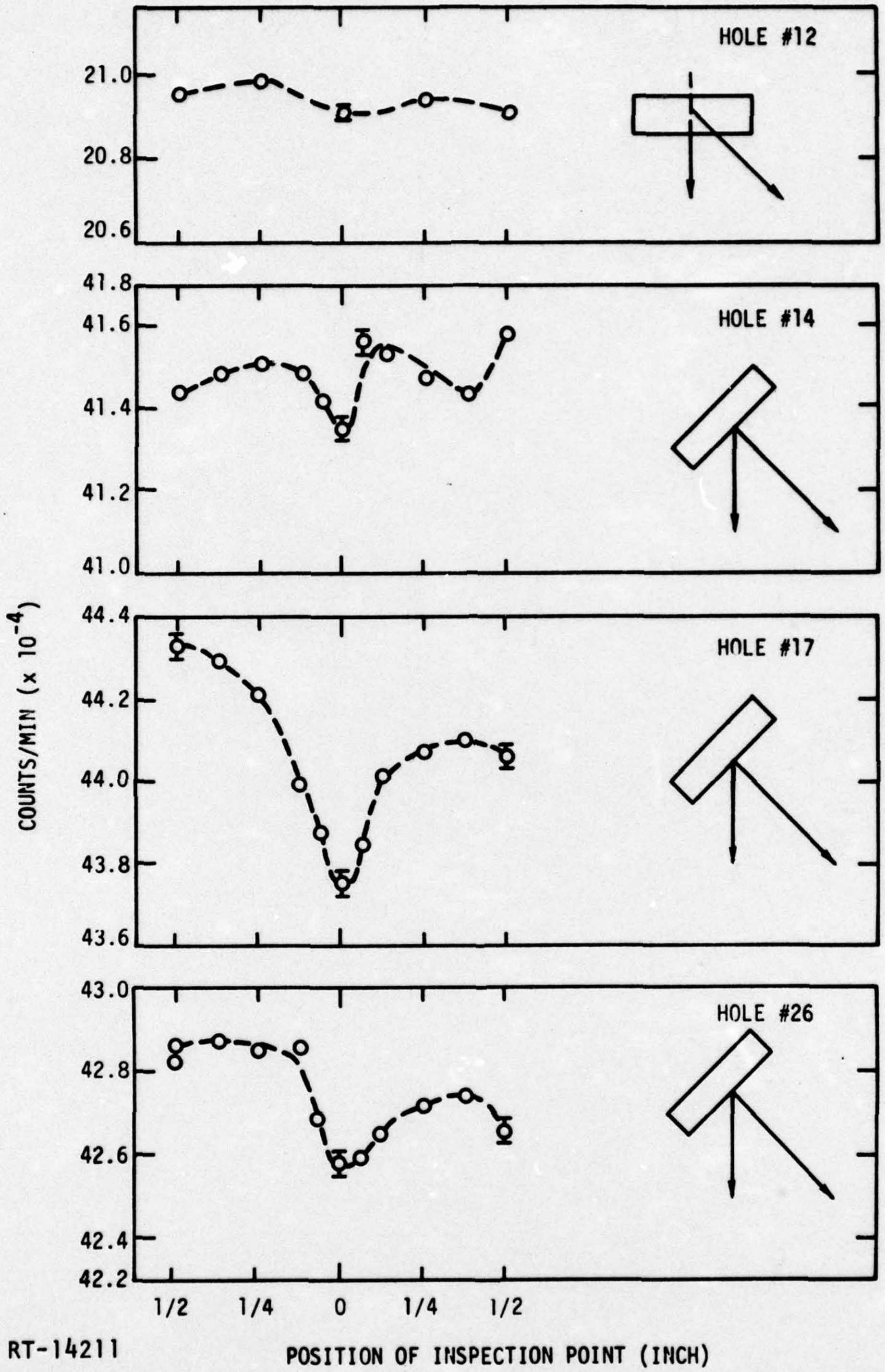

Figure 30. Response of the photon scattering gauge to holes 12, 14, 17, and 21 at one depth each

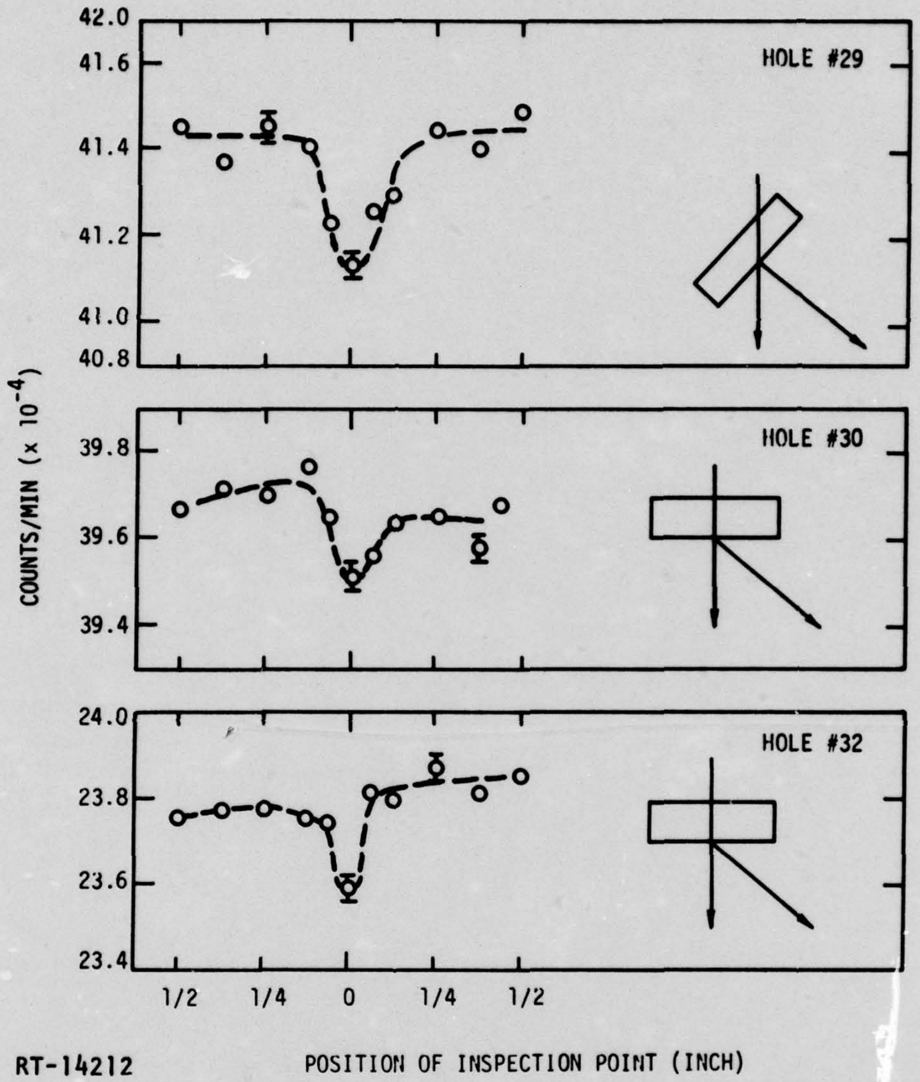

Figure 31. Response of the photon scattering gauge to holes 29, 30, and 32 at one depth each

the focal point relative to the hole. The data points reflect the total number of detector counts per minute at each position of the inspection volume element, without any correction for contributions from background or secondary scattering radiations. Even though such a correction would increase the magnitude of the fractional response deflection due to a hole, it would not in any way improve the statistical precision of the measured deflection. In other words, if the magnitude of the deflection is expressed in terms of the number of standard deviations of the data points, there is no improvement for the case of the corrected net response.

Also displayed with the response to each hole is a schematic representation of the sample orientation selected for the measurement.

Studying the gauge response to each hole in some detail, it is apparent from Figure 28 that the presence of hole 1 is clearly discernible. The pronounced slope in the nondefect part of the response is thought to be due to the fact that sample S_3 was slightly out of round. The resulting effect on the measurement was that the upper edge of the sample experienced a slight vertical displacement as the sample was rotated. This vertical change caused a slight variation to take place in the length of travel through the sample of the exiting beam on its way to the detector. This, in turn, resulted in a change of absorption experienced by the exiting beam. The fact remains, however, that despite this change in sample position the hole is clearly discernible as a highly localized response deflection.

The response to hole 5 was measured in three different places; 0.25, 0.375, and 0.500 inch, respectively, from the surface. As expected, there is no noticeable difference between the first two responses since the hole clearly extends through the inspection volume element in both cases. In the third case, however, the response deflection is greatly reduced, indicating that the inspection point is near the end of the hole. Since the coordinates for any inspection point are uniquely defined, the latter measurement pinpoints the location of the bottom of the hole. In a complete scan, in which data for the entire sample is available, the size, direction, and location of any defect are thus uniquely defined.

The response to hole 6 is quite pronounced. It also shows the out-of-round effect seen in the case of hole 1.

Hole 10 provides a clear example of how well the response to the holes can be defined if the data is taken in such a manner that the inspection point is moved right through the hole. As stated earlier, considerable effort was expended under the constraints imposed by the available equipment to optimize the response to hole 10. Since hole 10 is of the same size relative to the inspection volume element as holes 1 and 5, the response of the latter could be optimized to the same magnitude of deflection.

The response to hole 12 was not optimized since it was nearly impossible to physically locate the sample within the geometric system confines in an appropriate measurement position. In fact, in the case of hole 36, which is located on the same sample surface as 12, it was impossible to locate the hole in the beam.

The responses to the remaining holes, 14, 17, 26, 29, 30, and 32, all clearly show the presence of the hole. They are usually also subject to the out-of-found effect.

3.5 DISCUSSION OF RESULTS

All holes are clearly discernible in the gauge response. An exception is 36, for which the sample could not be placed in a suitable position because the gauge had been designed for a different type of sample configuration.

The smallest hole inspected is 14 with a clearly recognizable response deflection. It has about one-third the volume of 12, but was measured with a stronger response. This is further evidence of the fact that the sample could not be properly positioned for the scan of 12.

For the interpretation of the scans of hole 12 versus 14 and the multiple scans of 5, it has to be noted that for a hole longer than the length of the inspection volume element, but narrower than its width, the width of the hole is defined by the magnitude of response deflection. As the hole becomes big compared to the dimensions of the inspection volume

element, the response variation assumes a maximum value which is the same for any location within the hole. In fact, if the true net response were shown, corrected for background and secondary scattering effects, the response deflection would be 100% for as long as the inspection volume element fell completely within the hole.

From a quantitative point of view the response of hole 10 is analyzed since this is the only response which is close to demonstrating the true potential of the technique. Hole 10 was selected on a completely random basis. There are no geometric considerations favoring it over any of the other defects, except 12 and 36. The measured, uncorrected response of 10 shows a deflection of 2.2%, corresponding to 15 standard deviations, comparing very favorable to the theoretical prediction of 5% based on the ratio of void to inspection volumes. This demonstrates that the total response is not overly affected by background and secondary effects, thus easily lending itself to parametric projection. It also means that a 0.6% deflection would be clearly discernible as a 4-sigma deviation from the average response. It would correspond to a hole with a 0.016 inch diameter and a length of at least 0.125 inch.

If even smaller holes are to be detected, the inspection volume element must be reduced in size. For example, a halving of the length, width, and height of the inspection volume element would result in a volume reduction by a factor 8, which translates into an increase in resolution capability by a factor 8. In other words, continuing the discussion of the previous paragraph, a hole with a radius of 0.008 inch and a length of 0.016 inch, or one with a radius of 0.004 inch and a length of 0.064 inch would be seen as a 4-sigma response deflection.

It would be feasible to reduce the volume size of the inspection volume element by another factor 4 to 8, increasing resolution capability by roughly the same amount. Whether further reduction could be realized is not quite certain at this time. A study would have to determine if secondary scattering effects did not tend to put a practical lower limit to the amount of resolution that could be achieved. Such an improvement in resolution would, of course, result in a commensurate increase in the

number of data points that describe a given sample and, therefore, an increase in inspection time. The latter can be compensated to a degree by the selection of more intense radiation sources.

3.6 RECOMMENDATIONS

The photon scattering gauge results clearly indicate the power of this technique. The defects are discernible roughly within the theoretical prediction and a parametric projection showed that the resolution can be improved by a factor of between 32 and 64.

To further explore the feasibility of the projected resolution improvement, it is important to consider count rates and inspection times. A detailed quantitative parametric analysis in report INTEL-RT 6115-001, prepared under Contract DAAG46-76-C-0019 for the U. S. Army Materials and Mechanics Research Center (Ref 13), demonstrated that the feasibility demonstration unit could be projected into an optimized gauge with a total detector improvement factor of 1.5×10^4. In other words, the improved system would have a total combined count rate from an improved detector arrangement which was estimated to be 1.5×10^4 higher than the one achieved with the test bed. A further improvement of a factor 2.4, as described in the above report, is achieved by suitable three-dimensional data smoothing which improves the statistical significance of the data. In order to provide a quantitative framework for a projection of the potential of the photon scattering gauge for the flaw inspection of HIP components, it was assumed that the model underlying the referenced projection identically applies to this case. This assumption should be reasonable, since the referenced system has been used for measurements on a HIP sample. However, the space requirements of the HIP samples might be quite different from those of the 105-mm projectile sample used for the referenced report.

The combined improvement factor of $2.4 \times 1.5 \times 10^4 = 3.6 \times 10^4$ means that the total scan time of five minutes for the inspection of each hole would be reduced to 8.3 milliseconds. As mentioned earlier, the size of the inspection volume element for these measurements was 0.002 cubic inch, resulting in an estimated 18,000 data points for a complete scan. With a

measurement time of 8.3 milliseconds per data point a total scan time of 2.5 minutes would result.

If this hypothetical, improved system, which would have resolution characteristics identical to the ones applying to the test measurements, were altered by reducing the size of the inspection volume element by a factor 8 and keeping all other parameters unchanged, the following measurement time projection results.

a. A reduction of the inspection volume element by a factor 8 results in eight times as many inspection points. The total inspection time becomes eight times longer.

b. In order to reduce the size of the inspection volume element, the collimator dimensions have to be altered. This results in a total estimated effect of a decrease of the available count rate by a factor 8.

The total penalty is thus a factor of 8 x 8 = 64. This means that the total inspection time will grow from 2.5 minutes to 2.7 hours, unless the system is optimized for HIP samples and not for 105-mm projectiles.

In such an optimization, use would be made of the fact that a HIP sample similar to S_3 is of rather compact size and shape compared to a 105-mm projectile. The length of the latter results in a relatively inefficient detector arrangement which has to be confined to the sides of the projectile. An S_3 type sample, on the other hand, could practically be surrounded by a collimator-detector arrangement. The result would be an improvement in solid angle of the order of a factor 2. Thus, a total inspection time of roughly 1.4 hours per S_3 type sample would be expected from a system that would measure the presence of a hole 0.004 inch in diameter and 0.064 inch long at the 4-sigma level. This inspection time could be further decreased by utilizing a more intense radiation source.

It is important to note that a system optimized for the inspection of HIP samples would more fully utilize the source radiation than the present system by placing one inspection station on either side of the

source, rather than just on one. This factor was *not* included in the above projection. In other words, in terms of the most expensive component of a photon scattering gauge, the intense radiation source, another factor of two improvement is realized. Thus, per source, a throughput rate of two samples in 1.4 hours, or one sample in 0.7 hour is obtained. Further improvements may well be realized if maximum advantage is taken of the geometric characteristics of HIP samples.

On the basis of the positive results of the measurements conducted under the subject report and the fact that a quantitative, parametric projection to an optimized inspection system for HIP samples indicates that such a system appears to be feasible from a technical point of view, it is recommended that such a system be developed as a fully automated high-resolution inspection device. The photon scattering technique naturally lends itself to automation since it routinely provides a data set in which the density of every inspection point is uniquely correlated with its three-dimensional coordinates. Thus, the data analysis needs to be merely concerned with a direct evaluation of the density data and not with a sophisticated tomographic-type analysis, as required for all conventional transmission-type inspection techniques.

REFERENCES

1. Joseph John, V. J. Orphan, D. E. Rundquist, and R. Sharp, "Feasibility Study of Applying Neutron Radiography for Improved Maintenance Inspection of Naval Aircraft and Aircraft Components," IRT Corporation Technical Report INTEL-RT 6044-001, November 1, 1973.

2. Joseph John, D. E. Rundquist, and R. Sharp, "Application of Neutron-Radiography Techniques for Nondestructive Detection of Corrosion in Naval Aircraft and Aircraft Components," IRT Corporation Technical Report INTEL-RT 6044-002, March 15, 1974.

3. D. E. Rundquist, R. Sharp, and Joseph John, "Feasibility Evaluation of Real-Time Imaging for Neutron-Radiographic Inspection of Naval Aircraft," IRT Corporation Technical Report INTEL-RT 6072-001, August 1, 1974.

4. J. E. Larsen, D. E. Rundquist, J. Baltgalvis, and Joseph John, "Investigation of Neutron-Radiography Techniques for Corrosion Inspection of A-7 Nose Landing Gear," IRT Corporation Technical Report INTEL-RT 6071-001, August 6, 1974.

5. J. E. Larsen, J. Baltgalvis, F. Patricelli, M. Gallardo, and Joseph John, "Evaluation of a Portable Neutron-Radiographic System for the Detection of Hidden Corrosion in the Wing Fuel Tank of the E-2C Aircraft," IRT Corporation Technical Report INTEL-RT 6082-001, February 25, 1975.

6. J. E. Larsen, R. Parks, J. Baltgalvis, and Joseph John, "Investigation of Neutron-Radiographic Techniques for Maintenance Inspection of Air Force Aircraft," IRT Corporation Technical Report INTEL-RT 6081-001, March 3, 1975.

7. F. Patricelli, J. E. Larsen, J. Baltgalvis, R. Parks, and Joseph John, "Californium-252 Based Neutron Radiography for the Detection of Disbonds in the Spar Closure Area of 540 Series Helicopter Blades," IRT Corporation Technical Report INTEL-RT 6085-001, February 28, 1975.

8. Joseph John, "Mobile Neutron-Radiography System for Aircraft Inspection," Text of paper presented at Air Transport Association of America Nondestructive Testing Subcommittee Meeting, Houston, Texas, September 11-13, 1973, IRT Corporation Technical Report RT-TB-151.

9. F. Patricelli, J. E. Larsen, J. Baltgalvis, and Joseph John, "Experimental Evaluation of Neutron Radiography for Quantitative Determination of Corrosion in Aircraft Structure," IRT Corporation Technical Report INTEL-RT 6093-001, January 28, 1976.

10. H. Harper, J. Baltgalvis, H. Weber, and Joseph John, "Quantitative Determination of Corrosion Using Neutron Radiography," IRT Corporation Technical Report INTEL-RT 6119-001, July 30, 1976.

11. Joseph John, J. E. Larsen, F. Patricelli, H. Harper, and J. Baltgalvis, "Neutron Radiography for Maintenance Inspection of Military and Civilian Aircraft," IRT Corporation Technical Report INTEL-RT 4421-002, presented at International Symposium on Californium-252 Utilization, held at Commissariat a l'Energie Atomique, Centre d'Etudes Nucleaires de Saclay, France, April 26-28, 1976.

12. Joseph John, "Californium-Based Neutron Radiography for Corrosion Detection in Aircraft," Practical Applications of Neutron Radiography and Gauging, ASTM STP 586, American Society for Testing and Materials, 1976, pp. 168-180.

13. H. Weber, J. C. Young, D. Costello, W. E. Gober, and Joseph John, "Fully Automated System for Inspection of Explosive Charge of 105-mm M-1 Projectiles Under the U. S. Army's Ammunition Base Modernization Program," IRT Corporation Technical Report INTEL-RT 6115-001, January 7, 1976.

DISTRIBUTION LIST

No. of Copies	To
	Commander; US Army Aviation Systems Command; PO Box 209; St. Louis, Missouri 63166
10	ATTN: DRSAV-EXT
1	ATTN: DRSAV-FE (Cliff Sims, Maint. Engr.)
1	ATTN: DRSAV-EQ (C. Crawford, Sys Dev & Qual)
1	ATTN: DRSAV-FES (H. Bull, Corpus Christi)
2	ATTN: DRSAV-ZDR (Ref Library)
1	ATTN: DRSAV-LEP (D. Fleming)
1	Project Manager; Advanced Attack Helicopter; ATTN: AMCPM-AAH, TM; PO Box 209; St. Louis, Missouri 63166
1	Project Manager; Utility Tactical Transport Aircraft System; ATTN: AMCPM-UA-T; PO Box 209, St. Louis, Missouri 63166
1	Project Manager; CH-47 Modernization; ATTN: AMCPM-CH47M; PO Box 209; St. Louis, Missouri 63166
1	Project Manager; Advanced Scout Helicopter; ATTN: AMSAV-SIA, PO Box 209; St. Louis, Missouri 63166
1	Product Manager; Aircraft Survivability Equipment; ATTN: AMCPM-ASE-TM; PO Box 209, St. Louis, Missouri 63166
1	Product Manager; Cobra; ATTN: AMCPM-CO-T; PO Box 209; St. Louis, Missouri 63166
1	Product Manager; Iranian Aircraft Program; ATTN: AMCPM-IAP-T; PO Box 209, St. Louis, Missouri 63166
4	Commander; US Army Materiel Command; ATTN: AMCRD-TE; 5001 Eisenhower Avenue; Alexandria, Virginia 22333
1	Director; Eustis Directorate; US Army Air Mobility R&D Lab; ATTN: SAVDL-EU-TAS; Ft. Eustis, Virginia 23604 (Mr. Haselbauer)
1	Director; Ames Directorate; US Army Air Mobility R&D Lab; ATTN: SAVDL-AM; Ames Research Center; Moffett Field, California 94035 (Mr. Andre)
1	Director; Langley Directorate; US Army Air Mobility R&D Lab; ATTN: SAVDL-LA; Mail Stop 266; Hampton, Virginia 23365
1	Director; Lewis Directorate; US Army Air Mobility R&D Lab; ATTN: SAVDL-LE; 21000 Brookpark Road; Cleveland, Ohio 44135

No. of Copies	To
	Director; US Army Materials & Mechanics Research Center; Watertown, Massachusetts 02172
1	ATTN: AMXMR-PT (Mr. Fahey)
1	ATTN: AMXMR-MQ
1	Director; Production Equipment Agency; Rock Island Arsenal; ATTN: AMXPE-MT; Rock Island, Illinois 61201
	Air Force Materials Laboratory; Manufacturing Technology Division; Wright-Patterson Air Force Base, Ohio 45433
1	ATTN: AFML/LTM
1	ATTN: AFML/LTN
1	ATTN: AFML/LTE
1	Commander; US Army Electronics Command; Ft. Monmouth, New Jersey ATTN: AMSEL-RD-P
1	Commander; US Army Missile Command; Redstone Arsenal, Alabama 35809; ATTN: AMSMI-IIE
1	Commander; US Army Troop Support Command; 4300 Goodfellow Blvd.; St. Louis, Missouri 63120; ATTN: AMSTS-PLC
1	Commander; US Army Armament Command; Rock Island, Illinois 61201 ATTN: AMSAR-PPR-1W
1	Commander; US Army Tank-Automative Command; Warren, Michigan 48090 ATTN: AMSTA-RCM.1
12	Commander; Defense Documentation Center; Cameron Station; Building 5; 5010 Duke Street; Alexandria, Virginia 22314
2	Hughes Helicopter; Division of Summa Corporation; ATTN: Mr. R. E. Moore, Bldg. 314; M/S T-419; Centinella Avenue & Teale Street; Culver City, California 90230
2	Sikorsky Aircraft Division, United Aircraft Corporation; ATTN: Mr. Stan Silverstein; Section Supervisor, Manufacturing Tech.; Stratford, Connecticut 06497
2	Bell Helicopter Co.; ATTN: Mr. P. Baumgartner, Chief, Manufacturing Technology; PO Box 482, Ft. Worth, Texas 76101
2	Kaman Aerospace Corp.; ATTN: Mr. A. S. Falcone, Chief of Materials Engineering; Bloomfield, Connecticut 06002
2	Boeing Vertol Company; ATTN: R. Pinckney, Manufacturing Technology; Box 16858, Philadelphia, Pennsylvania 19142

No. of Copies	To
2	Detroit Diesel Allison Division, General Motors Corporation; ATTN: James E. Knott; General Manager; PO Box 894; Indianapolis, Indiana 46206
2	General Electric Company; ATTN: Mr. H. Franzen; 10449 St. Charles Rock Road; St. Ann, Missouri 63074
2	AVCO-Lycoming Corporation; ATTN: Mr. V. Strautman, Manager Process Technology Laboratory; 550 South Main Street, Stratford, Connecticut 08497
2	United Technologies Corporation; Pratt & Whitney Aircraft Division; Manufacturing Research and Development; ATTN: Mr. Ray Traynor; East Hartford, Connecticut 06108